

Multifragmentation *vs.* Evaporation *vs.* Binary-Decay in Fragment Production

S. G. Mashnik¹, K. K. Gudima², M. I. Baznat²,

¹X-3, Los Alamos National Laboratory, Los Alamos, New Mexico 87545, USA

²Institute of Applied Physics, Academy of Science of Moldova, Chişinău, Moldova

Abstract

This paper presents part of an internal LANL Progress Report on completion of the “S” and “G” versions of the improved Cascade-Exciton Model (CEM03.01) and the Los Alamos Quark-Gluon String Model (LAQGSM.03.01) codes. The “S” versions consider fragmentation of compound nuclei produced after the preequilibrium stage of reactions for excitation energies above $2 \times A$ MeV using the Statistical Multifragmentation Model (SMM) by Botvina *et al.* (“S” stands for SMM), while the “G” versions describe evaporation/fission stages of reactions using the fission-like binary-decay model GEMINI of Charity *et al.* (“G” stands for GEMINI) instead of using the the Generalized Evaporation Model GEM2 of Furihata incorporated into the standard versions of these codes. We present here an analysis of the recent 660 MeV p + ¹²⁹I and 3.65 GeV p + ¹¹²Sn JINR measurements, of the new COSY data on 1.2 GeV p + (13 nuclei from Al to Th), of the 300 MeV and 1 GeV p + ⁵⁶Fe data measured at GSI in inverse kinematics, and of the new GSI data on 1 GeV/nucleon ¹²⁴Xe and ¹³⁶Xe + Pb. To better understand the mechanisms of fragment production, we discuss several calculated but not-yet-measured kinematic characteristics of products of these reactions, which are predicted to be quite different by SMM, GEMINI, and GEM2. We find these kinematic quantities to be potentially useful in differentiating these reaction mechanisms if they can be measured in future experiments.

1. Introduction

For Proton Radiography (PRAD) as a radiographic probe for the Advanced Hydro-test Facility and other LANL applications, we have developed recently (see, *e.g.*, [1]–[4] and references therein) improved versions of the Cascade-Exciton Model (CEM) [5] and of the Los Alamos Quark-Gluon String Model (LAQGSM) [6] codes as event generators to be used in MCNP6, MARS, and MCNPX transport codes.

The latest versions of the event generators, CEM03.01 and LAQGSM03.01, [7]–[9] have significantly improved IntraNuclear Cascade (INC) models, updated preequilibrium, Fermi break-up, and coalescence models able to describe better than their predecessors emission of complex particles and light fragments, and were extended to describe photonuclear reactions up to tens of GeV. On the whole, CEM03.01 and LAQGSM03.01 describe nuclear reactions much better than their predecessors and other similar codes available to the nuclear physics community. They have been benchmarked on a variety of particle-particle, particle-nucleus, and nucleus-nucleus reactions at energies from 10 MeV to 800 GeV per nucleon, and have been or are being incorporated as event generators into the transport codes MCNP6, MARS, and MCNPX.

However, both CEM03.01 and LAQGSM03.01 still have some problems in providing an accurate description of light- and medium-mass fragments produced from some nuclear reactions

on intermediate-mass targets, which cannot fission or fragment into many channels using the GEM2 model. We address this problem in two different ways [10]:

1) By implementing into CEM03.01 and LAQGSM03.01 the Statistical Multifragmentation Model (SMM) by Botvina *et al.* [11]–[15], to consider multifragmentation as a mode competitive to evaporation of particles and light fragments, when the excitation energy U of a compound nucleus produced after the preequilibrium stage of a reaction is above $2 \times A$ MeV. This way, we have produced the “S” version of our codes (“S” stands for SMM), CEM03.S1 and LAQGSM03.S1.

2) By replacing the Generalized Evaporation Model GEM2 of Furihata [16]–[18] used in CEM03.01 and LAQGSM03.01 with the fission-like binary-decay model GEMINI of Charity *et al.* [19]–[23] which considers production of all possible fragments. This way, we have produced the “G” version of our codes (“G” stands for GEMINI), CEM03.G1 and LAQGSM03.G1.

The INC, preequilibrium, Fermi break-up, evaporation, fission, and coalescence models used in the current versions of our codes are described in detail in [4, 6, 7, 9] and references therein, while SMM and GEMINI incorporated into the “S” and “G” versions, are described in the original publications [11]–[15] and [19]–[23], respectively.

2. Results

We have incorporated into CEM03.01 and LAQGSM03.01 GEMINI and SMM as provided to us by their authors, Prof. Charity and Dr. Botvina, without any essential changes to or fitting of their parameters. A few “cosmetic” changes were made only to accommodate them to our FORTRAN compilers and to fix several observed “bugs”.

The upper-left plot in Fig. 1 shows the recent experimental data [24] on the mass-number distribution of the product yield from the reaction 660 MeV $p + {}^{129}\text{I}$ compared with results by the standard version of our CEM03.01 event generator, as well as with results by our new “S” and “G” codes (similar results are obtained for this reaction with LAQGSM03.01 and its “S” and “G” versions). One can see that the standard versions do not describe production of isotopes with mass number $26 < A < 63$ from this reaction observed in the experiment [24]. These products are too heavy to be evaporated from compound nuclei and the target is too light to fission, producing these isotopes as fission fragments (CEM03.01 and LAQGSM03.01 consider only “conventional” fission of preactinides and actinides and do not consider at all fission of nuclei with $Z < 65$).

The “S” and “G” versions do predict such isotopes and agree reasonably well with available experimental data. This is the main reason we have developed the “S” and “G” versions of our codes. The results by the “S” version for the A -distribution of product yield are very similar to the ones from the “G” version for the entire range of product masses, except the region of light fragments $10 < A < 20$, where there are no experimental data. From this plot we see only that products with $26 < A < 63$ are produced in this reaction and they can be described either via fission-like binary decays (the “G” versions of our codes), or as products of multifragmentation of highly-excited nuclei (the “S” versions), without a distinctive preference.

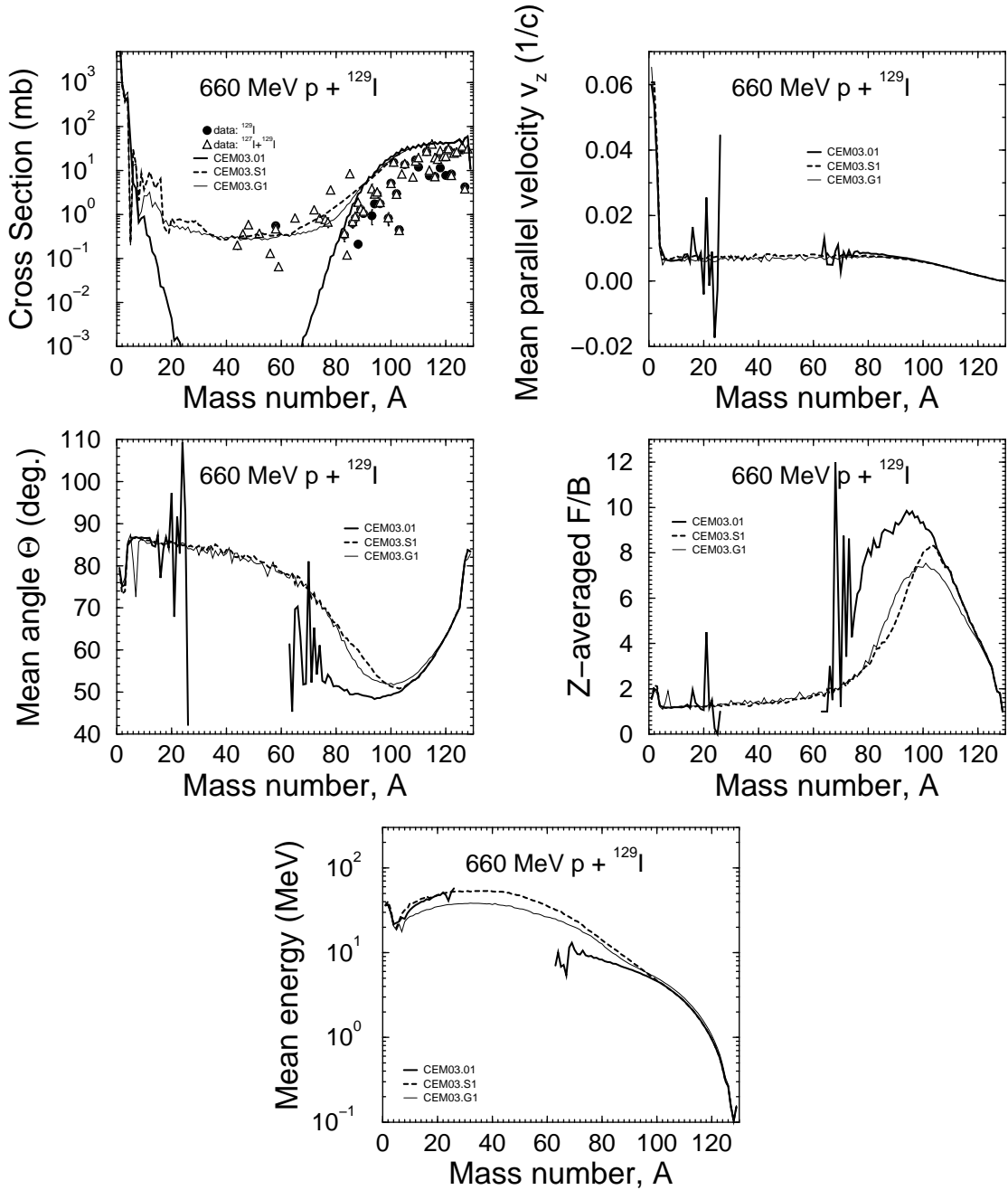


Figure 1: Predictions of CEM03.01, CEM03.S1, and CEM03.G1 for the mass number distribution of the product yield, mean parallel velocity v_z , mean production angle Θ , Z-averaged A-dependence of the F/B ratio of the forward product cross sections to the backward ones, and the mean kinetic energy of all products in the laboratory system for the reaction $660 \text{ MeV p} + {}^{129}\text{I}$ (lines) compared with available experimental data (symbols) [24], as indicated. The big fluctuations in the values by CEM03.01 of $\langle v_z \rangle$, $\langle \Theta \rangle$, $\langle R = F/B \rangle$, and $\langle T_{kin} \rangle$ for masses around $A = 20$ and 65 do not provide real physical information, as they are related to the limited statistics of our Monte-Carlo simulation caused by the very low yield of isotopes at the border between spallation and fragmentation, and at that between fragmentation and evaporation (with no events at all in the fragmentation region, $26 < A < 63$, neglected by CEM03.01). Our calculation provides only a few (or even one) isotopes of a given A in these mass regions, and mean values for such events do not have any significance.

Hoping to understand better the mechanisms for the production of isotopes with $26 < A < 63$ and of other products as well, we also calculate with all versions of our codes several kinematic properties of products: the mean parallel velocity $\langle v_z \rangle$, the mean production angle $\langle \Theta \rangle$, Z-averaged A-dependence of the F/B ratio of the forward product cross sections to the backward ones $\langle R \rangle$, and the mean kinetic energy of all products in the laboratory system, $\langle T_{kin} \rangle$, showed in other subplots of Fig. 1. Such characteristics can be measured with some specific techniques for some nuclear reactions and have proven to be very useful in understanding reaction mechanisms [4], although the activation technique of the experiment [24] does not provide such measurements. There are big differences among results provided by the standard version CEM03.01, and the “S” and “G” versions for $\langle \Theta \rangle$, $\langle R \rangle$, and $\langle T_{kin} \rangle$ for products with $70 < A < 100$. There is also a significant difference between predictions by the “S” and “G” version for $\langle \Theta \rangle$ of products with $85 < A < 110$, for $\langle R \rangle$ of the same products, and for $\langle T_{kin} \rangle$ of products with $15 < A < 80$. Unfortunately, none of these characteristics have been measured, so we cannot choose a specific reaction mechanism based on these results.

Fig. 2 shows results similar to the ones presented in Fig. 1, only for a lighter target, ^{56}Fe , and a lower energy of 300 MeV measured in inverse kinematics at GSI as 300 MeV/nucleon $^{56}\text{Fe} + p$ [25, 26]. The situation with the agreement or disagreement of our calculations with the data [25, 26] is very similar to that shown in Fig. 1, and all comments here are the same. The standard versions of our event generators strongly underestimate production of fragments with $A < 32$ from this reaction. These fragments can be described either via fission-like binary decays (the “G” versions of our codes), or as products of multifragmentation of highly-excited nuclei (the “S” versions). Comparing only the total production cross sections with experimental data (Fig. 2, for Z-integrated A-dependence of the yield, and Fig. 3, where we show cross sections of all measured isotopes, separately) does not allow us to identify the “real” nuclear reaction mechanisms for the production of these isotopes. Kinematic properties of products discussed above, like $\langle \Theta \rangle$, $\langle R \rangle$, and $\langle T_{kin} \rangle$ are different for different models and could shed more light on the mechanisms of these nuclear reactions, but such characteristics were also not measured in this experiment [25, 26]. In addition to the production cross section, the GSI inverse-kinematics technique provides also the mean parallel velocity v_z of all products in the reference frame of the projectile. Referring to the upper-right subplot of Fig. 2, $\langle v_z \rangle$ is not sensitive enough to the reaction mechanisms, and all three versions of our codes, “S”, “G”, and the standard version “03.01” provide almost the same $\langle v_z \rangle$, for this particular reaction. The mean kinetic energy of products is more sensitive to the reaction mechanisms considered, therefore more informative. As one can expect in advance, the multifragmentation mechanism (“S” version of our codes) provides more energetic light fragments (see the upper plots in Fig. 4, for $Z = 3, 6, 9, 12$, and 15) than the fission-like binary decay model GEMINI (“G” version) and the “conventional” evaporation model considered by our standard “03.01” version do. With increasing mass/charge of the products, this difference diminishes, and for isotopes with $Z \geq 20$, all three versions of our codes predict the same values of $\langle T_{kin} \rangle$ (lower plots in Fig. 4). Unfortunately, we do not have experimental data for these quantities, and therefore are not able to make an unambiguous choice between multifragmentation and binary decays in the production of light fragments from this reaction.

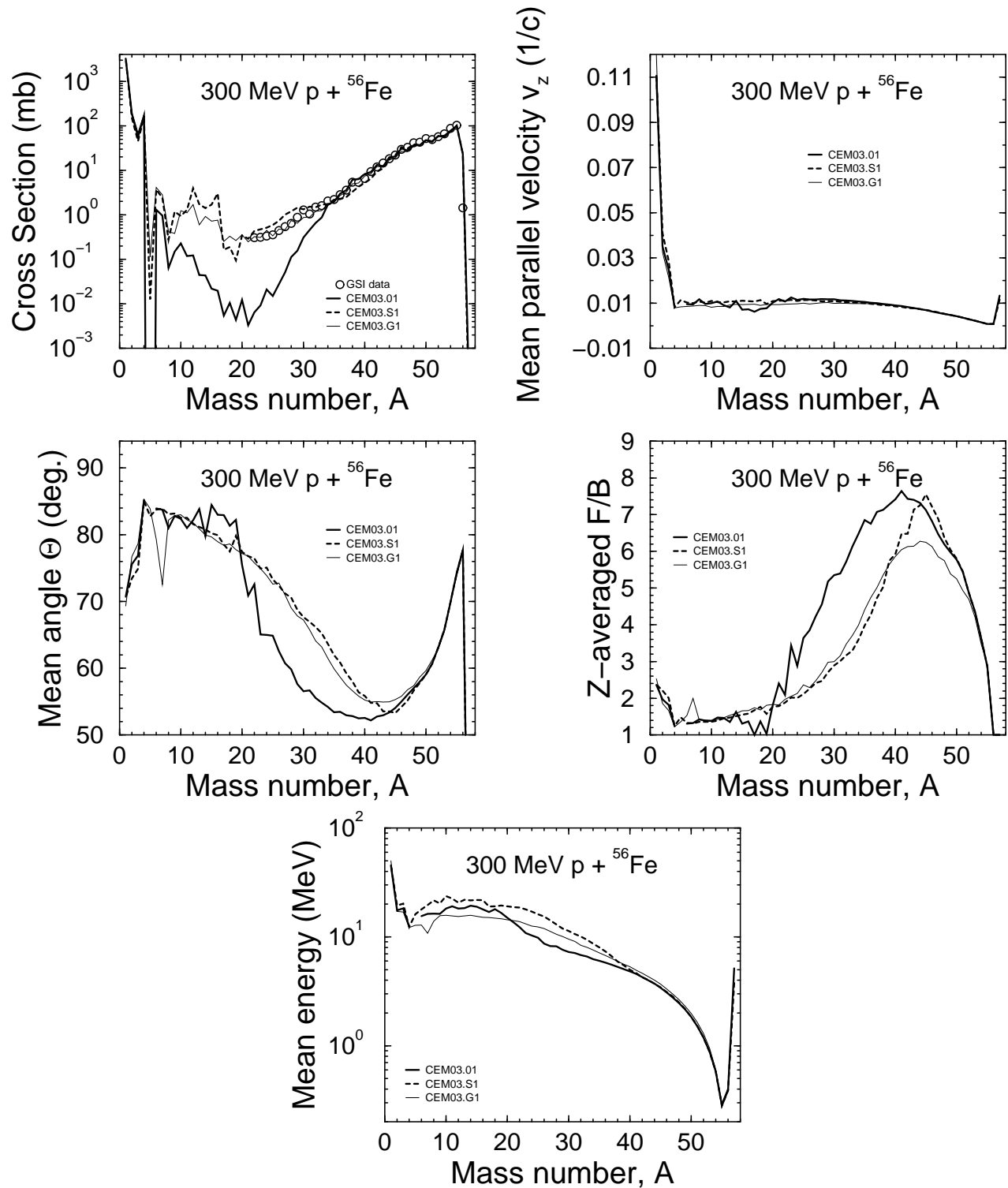


Figure 2: The same as Fig. 1, but for the reaction $300 \text{ MeV } p + {}^{56}\text{Fe}$ measured at GSI in inverse kinematics [25, 26].

300 MeV p + ^{56}Fe

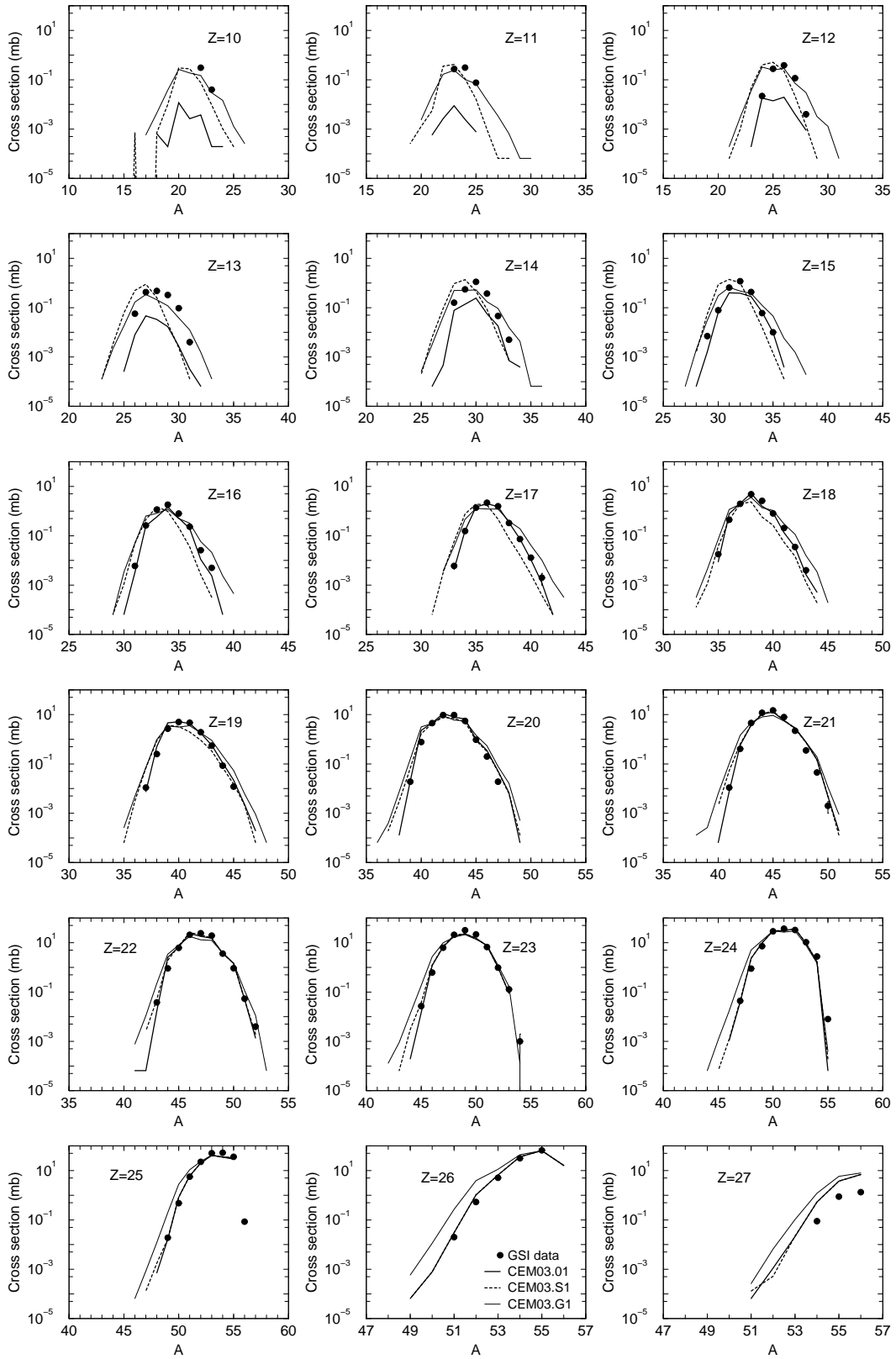


Figure 3: Comparison of all measured [25, 26] cross sections (symbols) of products from the reaction 300 MeV p + ^{56}Fe with CEM03.01, CEM03.S1, and CEM03.G1 results (lines), as indicated.

300 MeV p + ^{56}Fe

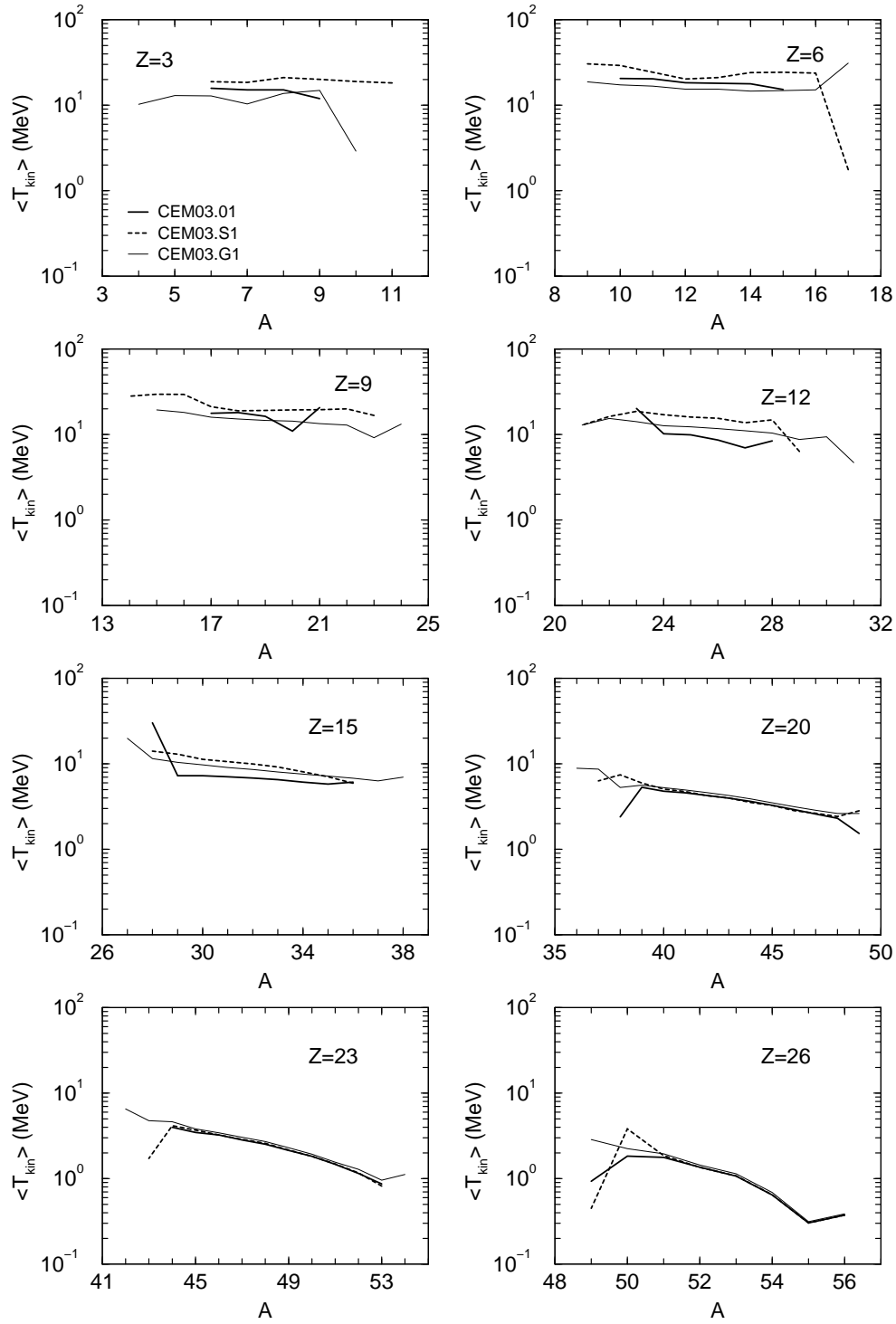


Figure 4: Predictions by CEM03.01, CEM03.S1, and CEM03.G1 for the mean kinetic energy of eight nuclides with $Z = 3, 6, 9, 12, 15, 20, 23,$ and 26 produced in the reaction $300 \text{ MeV p} + ^{56}\text{Fe}$ (no experimental data are available to us). The big fluctuations in the values of $\langle T_{kin} \rangle$ at both ends of distributions do not provide real physical information, as they are related to the limited statistics of our Monte-Carlo simulation caused by the very low yield of extremely neutron-rich and neutron-deficient isotopes. Our calculation provides only a few (or even one) isotopes of a given A in these regions, and mean values for such events do not have any significance.

Figs. 5–7 provide results for the same reaction and are similar to the ones shown in Figs. 2–4, but for a higher energy of 1 GeV, also measured in inverse kinematics at GSI by Carmen Villagrasa *et al.* [25, 26] and by Paolo Napolitani *et al.* [27, 28]. At 1 GeV (Figs. 5–7), the situation changes a little in comparison with what we have above at 300 MeV: The energy here is higher and the reaction is deeper, the target, ^{56}Fe , is not too heavy, so the standard version of our codes describe reasonably well all the measured product yields. At 1 GeV, the standard versions of our models predict light fragment production via deep spallation processes of the INC followed by preequilibrium and evaporation, without considering the multifragmentation (“S” version) or/and binary-decay processes (“G” version). It is interesting that at 1 GeV, the standard “03.01” event generators describe these cross sections measured at GSI even better than the “S” or “G” versions do, especially for products with $5 < A < 16$ (see the upper-left plot in Fig. 5) and $Z < 10$ (see Fig. 6). However, we consider this fact only as natural result of several years of careful development of our standard event generators rather than an indication that no multifragmentation and/or binary decays occur at 1 GeV (from a physical point of view, if we have multifragmentation and/or binary decays at 300 MeV, one may expect to have them even more pronounced at 1 GeV): Our standard event generators CEM03.01 and LAQGSM03.01 consider the INC, preequilibrium, evaporation, and the coalescence models for the production of isotopes from this reaction, and each of these models have their own parameters. These parameters have been adjusted, then fixed, while developing CEM03.01 and LAQGSM03.01 so that our codes describe as well as possible arbitrary nuclear reactions. The “G” and “S” versions are produced [10] without any fitting or adjustment of any parameters. We think that by adjusting and fitting the parameters of the “G” and “S” versions, one might obtain an agreement of their results for the production cross sections no worse than that provided by the standard versions of our codes. A difference would likely be observed for predictions of other characteristics of these reactions, like the kinematic properties of products discussed previously. In the framework of the versions we have so far, the biggest difference among results for this reaction by the “S”, “G”, and the standard “03.01” versions is for $\langle \Theta \rangle$ and $\langle R \rangle$ for products with $12 < A < 40$, for $\langle T_{kin} \rangle$ of products with $5 < A < 30$, with also quite a big difference in the Z -integrated A -dependence of the yield for light fragments with $5 < A < 18$ (see the upper-left subplot in Fig. 5).

The GEM2 evaporation/fission model [16]–[18] does not consider the angular momenta of the emitted particles, therefore the angular momenta of nuclei calculated at the INC and preequilibrium stages of reactions are not used at all and neglected in evaporation and fission processes. The same is true for the “S” version of our codes. On the other hand, GEMINI [19]–[23] does consider angular momenta of all products, so the “G” version of our codes can be used to study the effect of angular momentum in nuclear reactions. To reveal the effect of angular momentum, L , of the compound nucleus on the “recoil characteristics” $\langle \Theta \rangle$, $\langle R \rangle$, and $\langle v_z \rangle$ of the reaction studied here, we have performed additional calculations with the “G” version of our codes assuming angular momentum of all compound nuclei being equal to zero. Results of such a modification of CEM03.G1 are shown in Fig. 5 with thin dashed lines, to be compared with the solid thin lines showing results by CEM03.G1 considering the real angular momenta of all compound nuclei. We see that the effect of angular momentum, L , of the compound nucleus on results for $\langle \Theta \rangle$, $\langle R \rangle$, and $\langle v_z \rangle$ calculated by GEMINI in CEM03.G1 is more important for products with $12 < A < 46$, but is not very strong, on the whole.

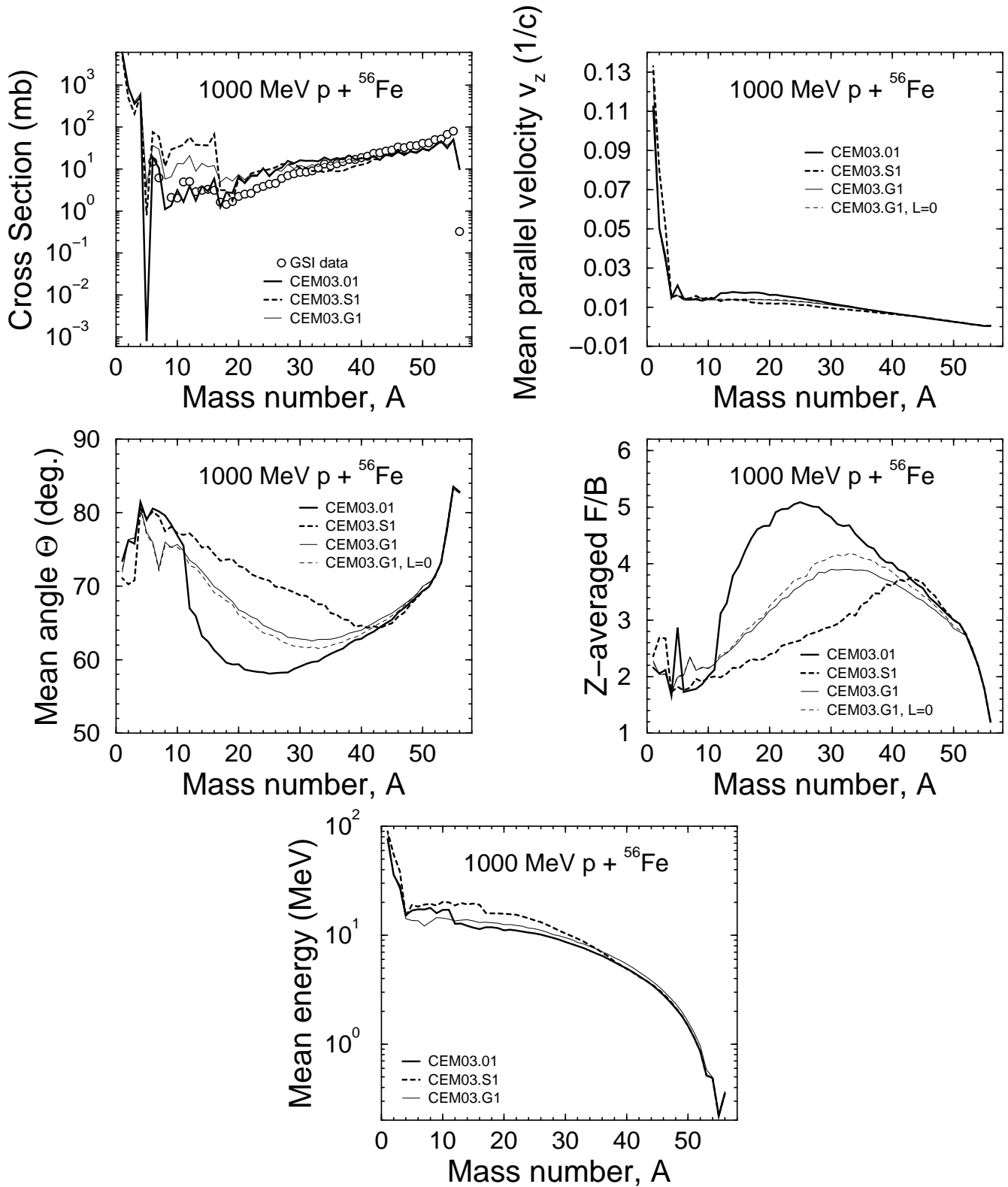


Figure 5: The same as Fig. 2, but for the reaction $1000 \text{ MeV } p + {}^{56}\text{Fe}$ measured at GSI in inverse kinematics by Villagrasa (medium and heavy products) [25, 26] and by Napolitani (light fragments) [27, 28] with coauthors. To reveal the effect of angular momentum, L , of the compound nucleus on results calculated by GEMINI in CEM03.G1, the dashed thin lines show results obtained assuming $L = 0$ in GEMINI, that should be compared with the results shown by thin solid lines obtained with real values of L .

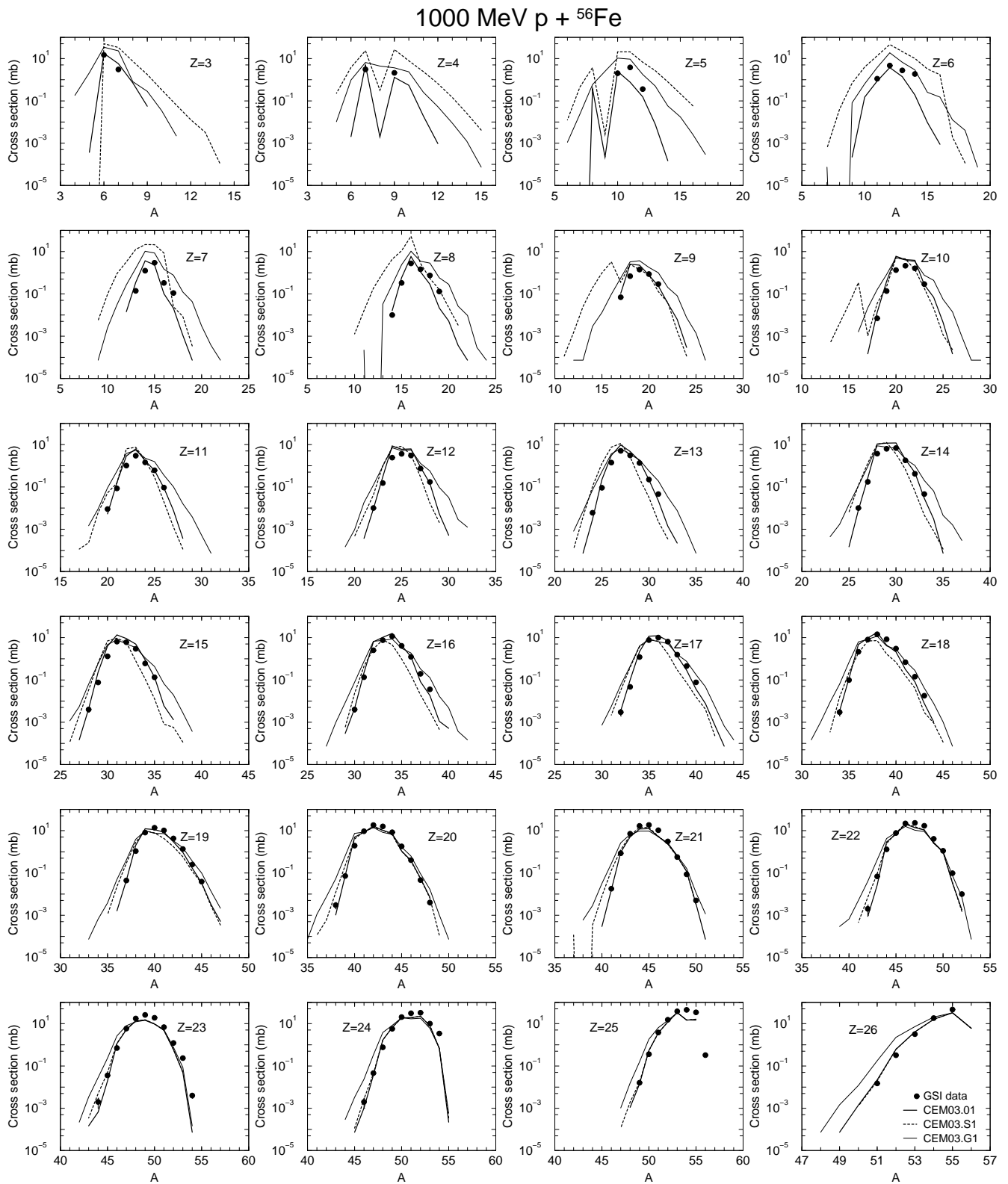


Figure 6: The same as in Fig. 3, but for the reaction 1000 MeV p + ^{56}Fe measured at GSI in inverse kinematics by Villagrasa (medium and heavy products) [25, 26] and by Napolitani (light fragments) [27, 28] with coauthors.

1000 MeV p + ^{56}Fe

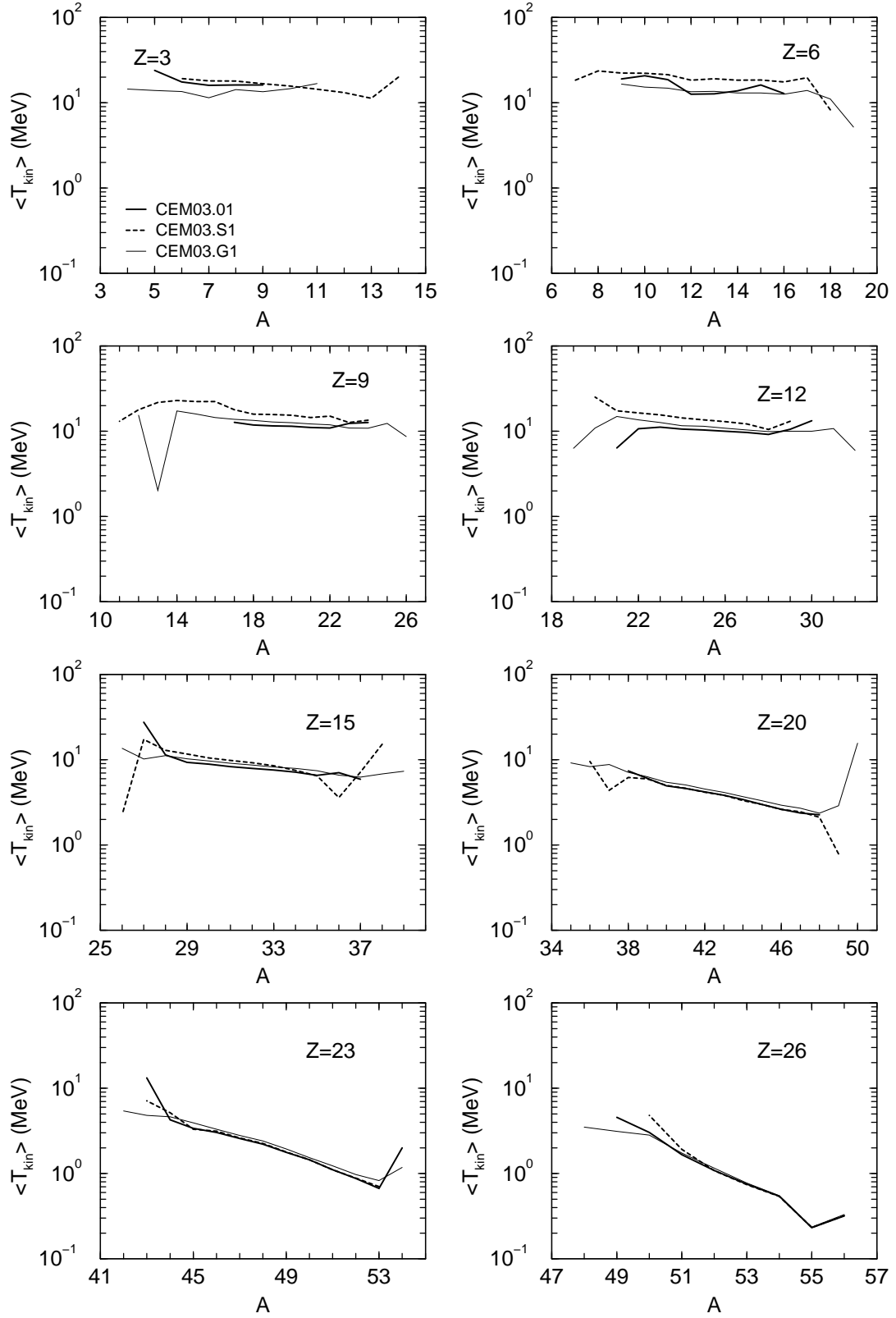


Figure 7: The same as Fig. 4, but for the reaction 1000 MeV p + ^{56}Fe .

Finally, Fig. 8 shows an example of a proton-induced reaction at a higher energy and a heavier target, namely, 3.65 GeV $p + {}^{112}\text{Sn}$, measured recently at JINR, Dubna with the activation technique [29]. The CEM03.01, CEM03.S1, and CEM03.G1 results shown in the figure present A -distributions of the yield of all products, *i.e.*, sums over Z of yields of all isotopes with a given mass number A , while the experimental data obtained by the activation method generally represent results for only some isotopes (sometimes, for only a single isotope) that contribute to the corresponding data point. That is, this comparison is only qualitative, not quantitative and provides only an approximate picture of the agreement between the calculations and measured data (just as in Fig. 1, where the data were also measured by the activation techniques at JINR). Activation measurements present the total yield for a given A only for cases when cumulative cross sections that include contributions from all precursors of all possible Z to the given measured yield; therefore, in general theoretical calculations of A -distribution of yields should be higher than many experimental activation data points. A much better, quantitative analysis would be to compare only the measured cross sections, isotope-by-isotope. Such a comparison of the measured data with results by CEM03.01 and LAQGSM03.01 (and by FLUKA and LAHET) is made in the original publication [29] and is not an aim of the present work. As the energy of the reaction shown in Fig. 8 is much higher than of all the other reactions shown in previous figures, the situation is also quite different. We see that the standard CEM03.01 predicts production of isotopes with all possible mass numbers, from 1 to 112. Intermediate isotopes with mass numbers $28 < A < 80$ are produced by CEM03.01 only via deep spallation, *i.e.*, the INC, followed by preequilibrium emission of particles up to ${}^4\text{He}$, followed by evaporation of particles and light fragments up to $A < 28$ from excited compound nuclei, without considering multifragmentation and/or binary decays. The “S” version considers production of such isotopes also via multifragmentation, while the “G” version, via binary decays. Nevertheless, the yield of products with $28 < A < 80$ predicted by the standard CEM03.01 model is higher than the ones predicted by both the “S” and “G” versions. Only for products with $5 < A < 28$ do the “S” and “G” versions predict a much higher yield than CEM03.01 does. For fragments with $8 \leq A \leq 16$, the “G” version predicts a yield about a factor of five higher than the standard CEM03.01, while the “S” version predicts even a higher yield, almost two orders of magnitude more than CEM03.01 does. Unfortunately, no experimental data for such products from this reaction are available presently, so the question about the “real” mechanisms for the production of such isotopes and their yields remains open.

Fig. 9 shows one example of proton spectra from 500 MeV $p + {}^{58}\text{Ni}$ calculated with our CEM03.01, CEM03.S1, and CEM03.G1 codes compared with experimental data by Roy *et al.* [30]. As one may expect in advance, all three versions of our codes provide very similar results, in a good agreement with the measurement. The spectra by “S” and “G” versions are a little lower in the energy range $T_p \simeq 25\text{--}50$ MeV in comparison with the standard version CEM03.01, but the difference is less than a factor of two, and there are no experimental data for this part of spectra, so again it is difficult to conclude which version works better here.

Figs. 10 and 11, compare results by CEM03.01, CEM03.S1, and CEM03.G1 for the total production cross sections of H, He, Li, and Be isotopes produced in interactions of 1.2 GeV protons with 13 target nuclei from Al to Th, measured just recently at the Cooler Synchrotron Facility COSY of the Forschungszentrum Jülich [31]. The experimental data shown in Figs. 10 and 11 are taken from Tables 4, 5, and 6 of Ref. [31] and present the measured production cross sections of H, He, Li, and Be isotopes only with kinetic energies below 100 MeV. We do not modify our codes to account for this experimental upper limit of the energy of detected

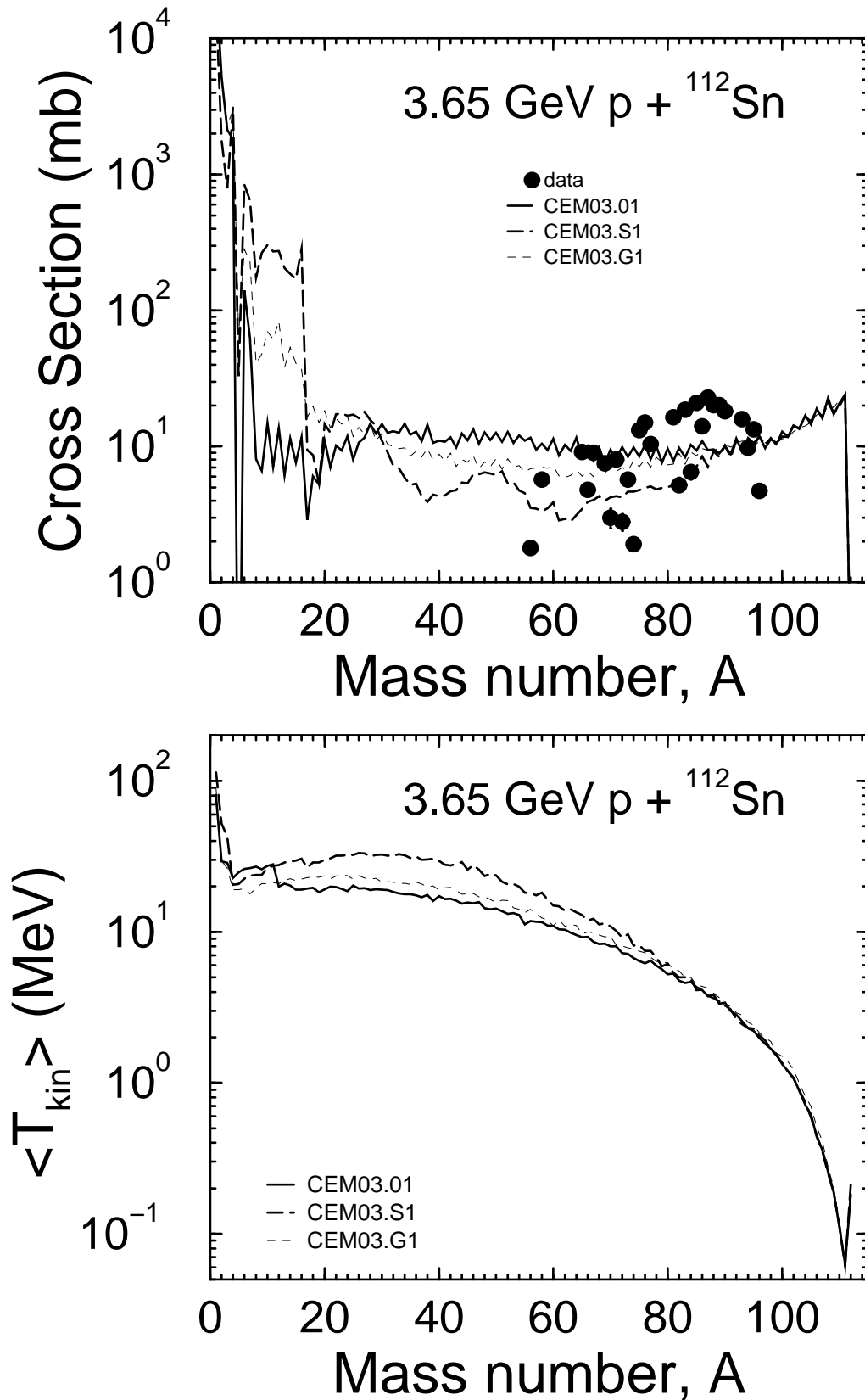


Figure 8: Predictions by CEM03.01, CEM03.S1, and CEM03.G1 for the mass number distribution of the product yield and the mean kinetic energy of all products in the laboratory system for the reaction $3.65 \text{ GeV p} + {}^{112}\text{Sn}$ (lines) compared with available experimental data (circles) [29], as indicated.

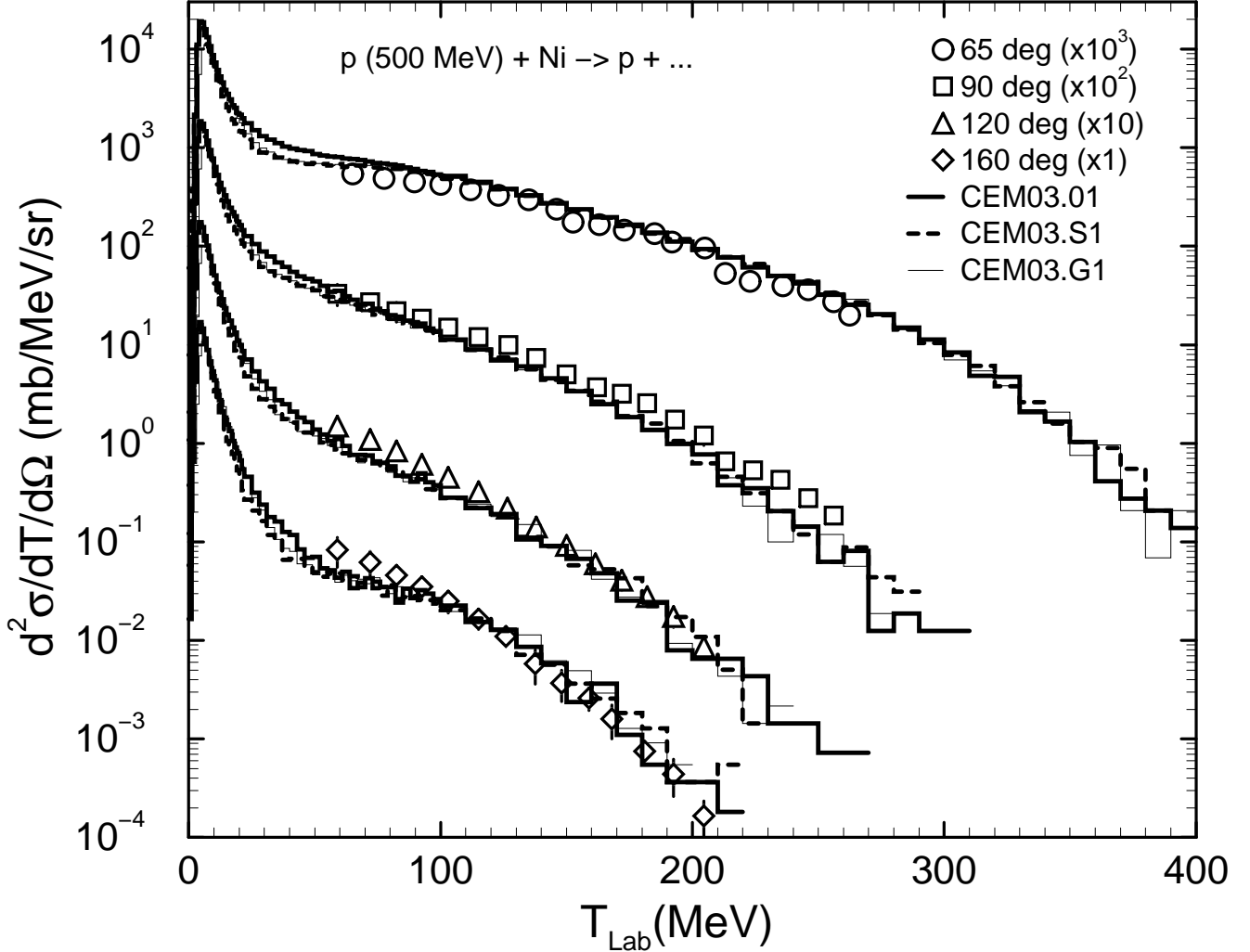


Figure 9: Experimental proton spectra from 500 MeV p + Ni [30] compared with CEM03.01, CEM03.S1, and CEM03.G1 results, as indicated.

particles; instead, we estimate the contributions from the high-energy tails ($T > 100$ MeV) of calculated spectra to the total calculated production cross sections. Fig. 12 shows an example of our estimates from angle-integrated energy spectra of p, d, t, ^3He , and ^4He calculated by CEM03.01 for the reaction 1.2 GeV p + Ag. The legend of this figure presents integrals of spectra (in mb) over the energy for particle energies above and below 100 MeV, respectively, and the percentage of contribution from high-energy tails ($T > 100$ MeV) of spectra to the total calculated cross sections. We see that for this particular reaction these contributions are rather small, of only about 17% for p, 3% for d, 1% for t, 2% for ^3He , and 0.4% for ^4He . Of course, for other targets and code versions, these contributions differ, but on the whole they remain small, limited to a few percent. This is why we can compare in Figs. 10 and 11 our total production cross sections calculated for all energies with experimental data that include energies only below 100 MeV.

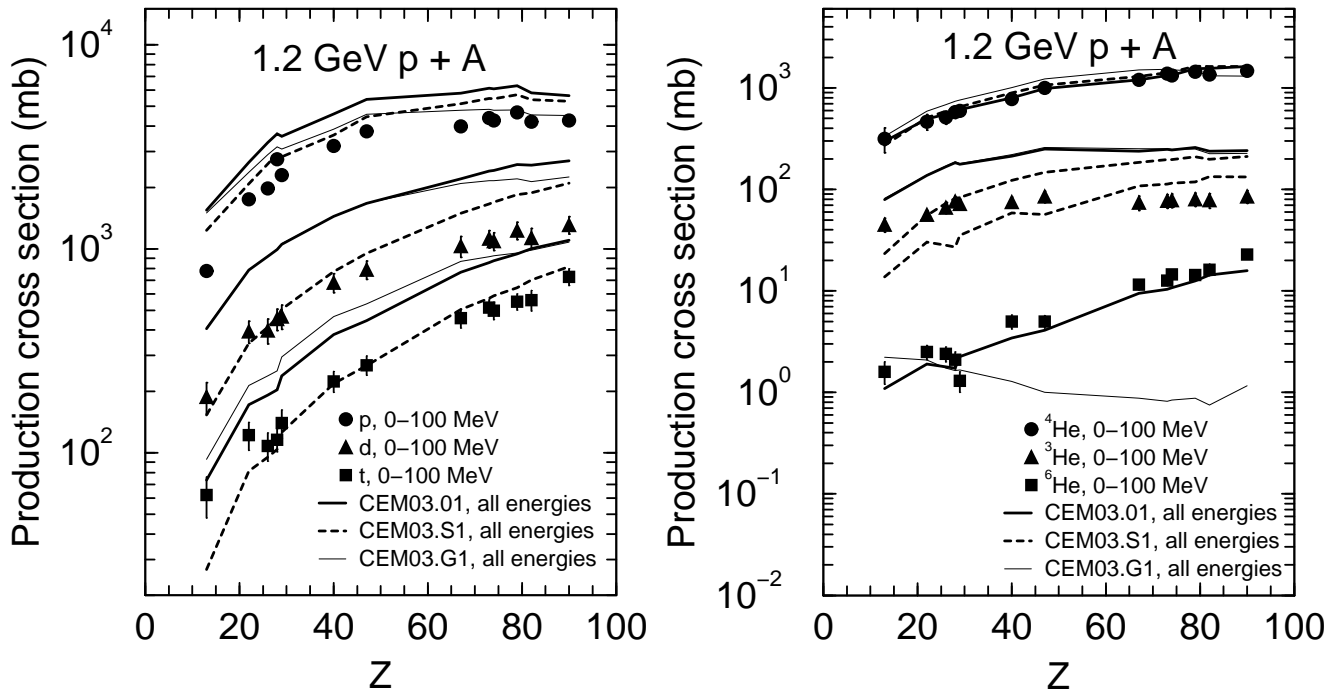


Figure 10: Comparison of measured [31] (symbols) production cross sections of hydrogen and helium isotopes with kinetic energies below 100 MeV for 1.2 GeV proton-induced reactions on thirteen targets between Al and Th with results from CEM03.01, CEM03.S1, and CEM03.G1 (lines), as indicated. Calculated results include contribution from products of all possible energies. An estimate of contribution from high-energy ($T > 100$ MeV) tails of calculated spectra to the total calculated production yields is shown in Fig. 12: It is of only about 17% for p, 3% for d, 1% for t, 2% for He3, and 0.4% for He4, in the case of Ag, using CEM03.01.

On the whole, with only a few exceptions, all versions of our codes describe reasonably the shape and the absolute values of the measured total production cross sections for all particles, from protons to ^{10}Be . The “S” version overestimates by several times the yields of all Li isotopes and of ^{10}Be from light and medium nuclei, the yields of ^7Be and ^9Be from all targets, and up to an order of magnitude the yields of ^6He from all targets. On the other hand, it agrees better than other versions of our codes with the data for all H as well as for ^3He and ^4He isotopes. The “G” version predicts reasonably well the yields of all H, all Be, ^3He , ^4He , ^6Li , ^7Li , and not so well for ^9Li isotopes, but the shape of the calculated lines for the yields of ^8Li , and especially of ^6He , disagrees with the data. On the whole, a better agreement with all measured data is observed for the standard version of our code, CEM03.01.

We now switch to analysis of several heavy-ion induced reactions with different versions of LAQGSM (CEM does not describe reactions induced by nuclei). Figs. 13 and 14 show a comparison of LAQGSM03.01, LAQGSM03.S1, and LAQGSM03.G1 results for the total production cross sections (yields) of nuclides with Z from 10 to 55 (all measured isotopes) produced from the fragmentation of ^{124}Xe in 1 GeV/A $^{124}\text{Xe} + ^{208}\text{Pb}$ collisions with the very recent GSI measurements [32]. Fig. 15 shows predictions for the mass-number distribution of the product yield and the mean kinetic energy (in the projectile frame of reference) of all products from the same reaction compared with available data [32].

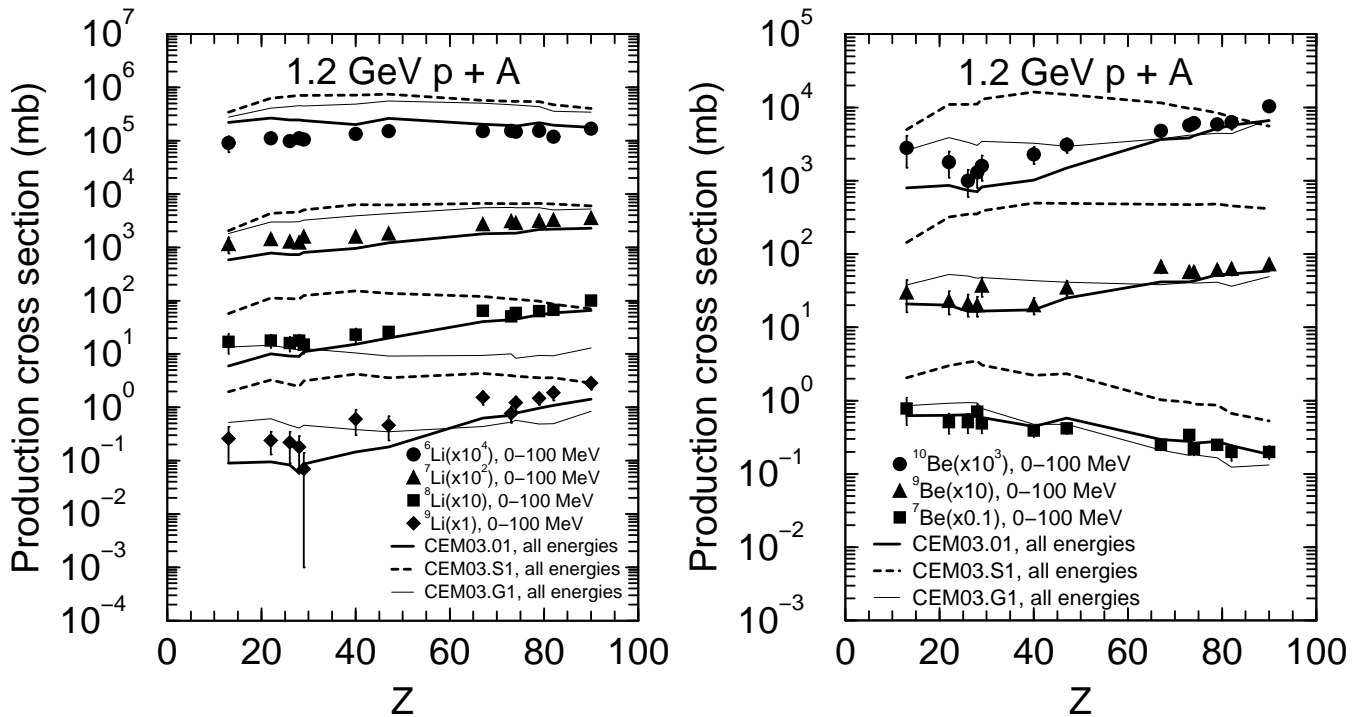


Figure 11: The same as Fig. 10, but for the production of Li and Be isotopes.

All versions of LAQGSM03.01 describe reasonably well cross sections for the production of all measured isotopes, from Neon to Cesium. A prediction by LAQGSM03.S1 of several unstable Neon isotopes with mass numbers lower than 18 not measured in the experiment (upper-left plot in Fig. 13) does not bother us much; these unstable isotopes should be disintegrated into stable nuclei. The transport codes using our event generators do take care of this; we could also add to the codes a check of such unstable products and disintegrate them before transferring their results to transport codes.

As observed above for proton-induced reactions, the standard version LAQGSM03.01 describes the production cross sections of all isotopes from 1 GeV/A $^{124}\text{Xe} + \text{Pb}$ on the whole a little better than the “S” and/or “G” versions do. We believe that the reason for this is the same as we had for proton-induced reaction: LAQGSM03.01 was developed carefully for several years; the nuclear reaction models incorporated into it were adjusted to each other and their parameters were fitted to describe as well as possible arbitrary reactions. The “S” and “G” versions of LAQGSM03.01 were developed [10] without any additional fitting or adjustment of any parameters. It would be possible to adjust the models of the “G” and “S” versions and to fit their parameters so that they describe production cross sections probably no worse than the standard version does, but this is outside the aim of the present work.

From comparison of only the measured [32] product yields with calculations by different versions of LAQGSM it is difficult, if not impossible, to uncover the “real” mechanisms of nuclear reactions contributing to the production of measured isotopes. In the upper plot of Fig. 15, we see a big difference between predictions by the standard, “S”, and “G” versions for the yields of isotopes with $15 < A < 31$, up to an order of magnitude and higher, but, unfortunately, these products were not measured [32]. We see also quite a big difference between the

predictions by different versions for the mean kinetic energy of products with $20 < A < 80$ (lower subplot in Fig. 15), but we do not have experimental data for this quantity either.

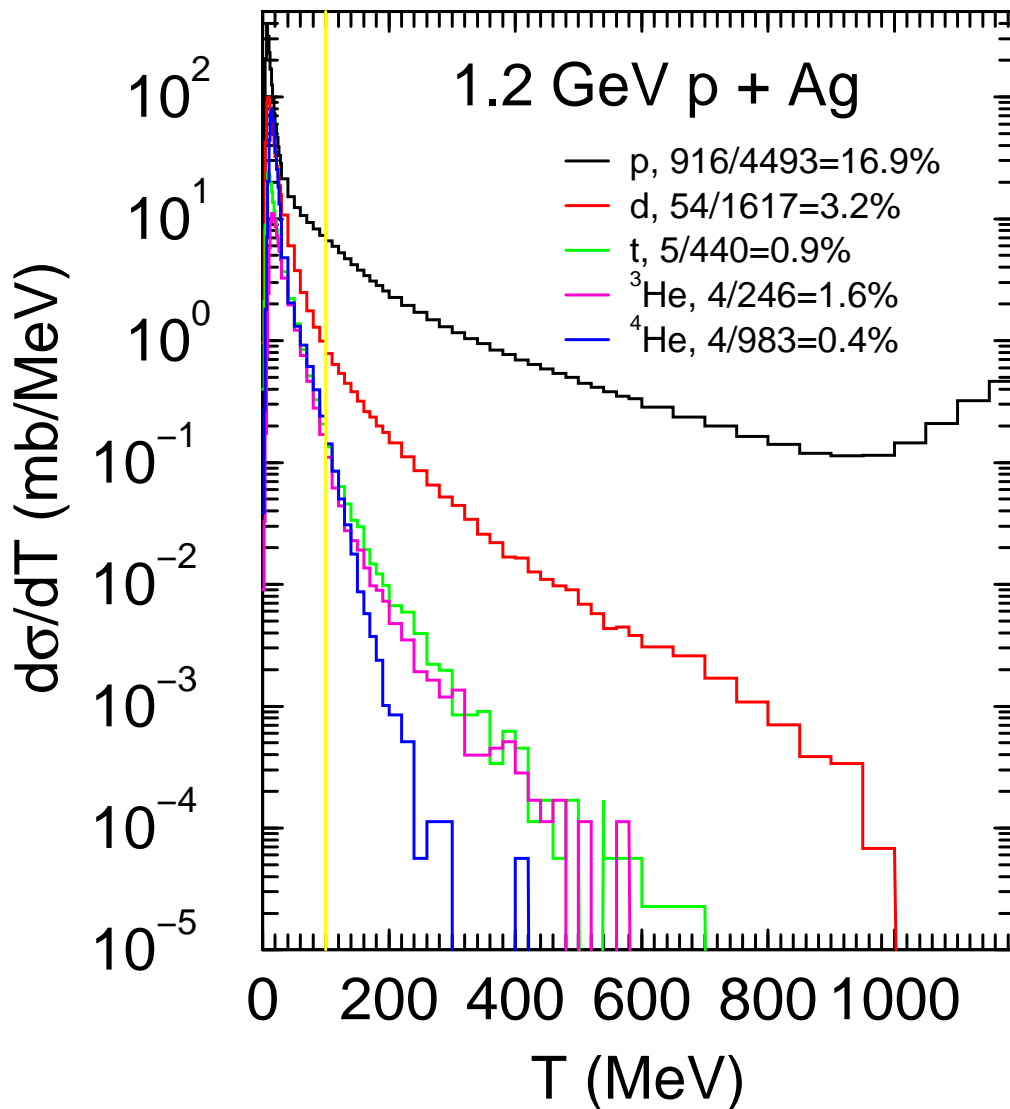


Figure 12: Angle-integrated energy spectra of p, d, t, ³He, and ⁴He emitted from the reaction 1.2 GeV p + Ag, as predicted by CEM03.01. The legend provides integrated production cross sections (in mb) for particles with energies above and below 100 MeV, respectively. These integrated cross sections are used to estimate the contributions from high energy ($T > 100$ MeV) tails of calculated spectra to the total calculated production yields. These contributions are about 17% for p, 3% for d, 1% for t, 2% for ³He, and 0.4% for ⁴He, for results by CEM03.01 for a Ag target.

1 GeV/A $^{124}\text{Xe} + ^{208}\text{Pb}$

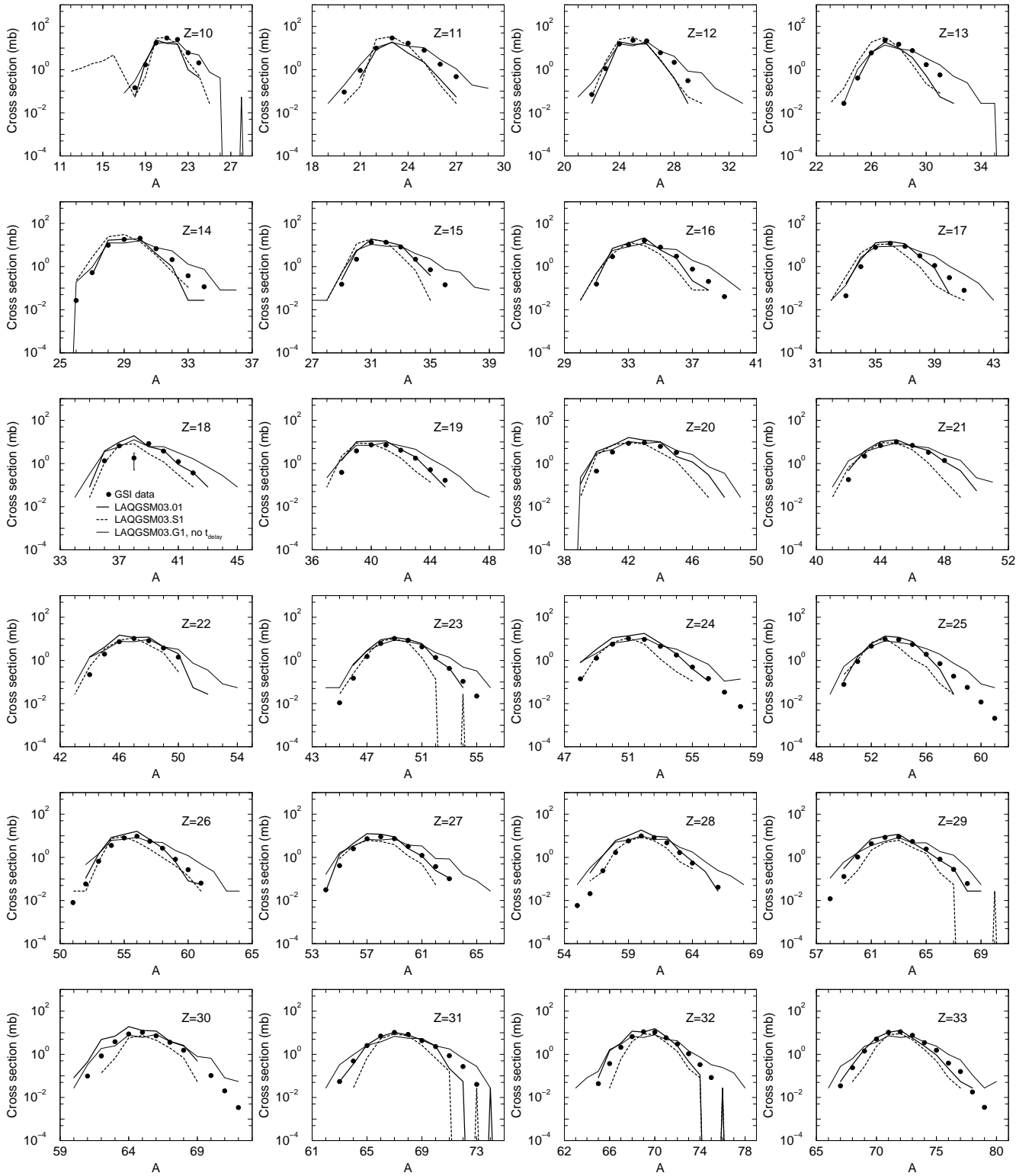


Figure 13: Comparison of LAQGSM03.01, LAQGSM03.S1, and LAQGSM03.G1 results (lines) for the total cross sections (yields) of nuclides with Z from 10 to 33 produced from fragmentation of ^{124}Xe in 1 GeV/A $^{124}\text{Xe} + ^{208}\text{Pb}$ collisions with the recent GSI measurements [32] (circles), as indicated. No delay time in GEMINI is considered in the LAQGSM03.G1 calculation of this reaction.

1 GeV/A $^{124}\text{Xe} + ^{208}\text{Pb}$

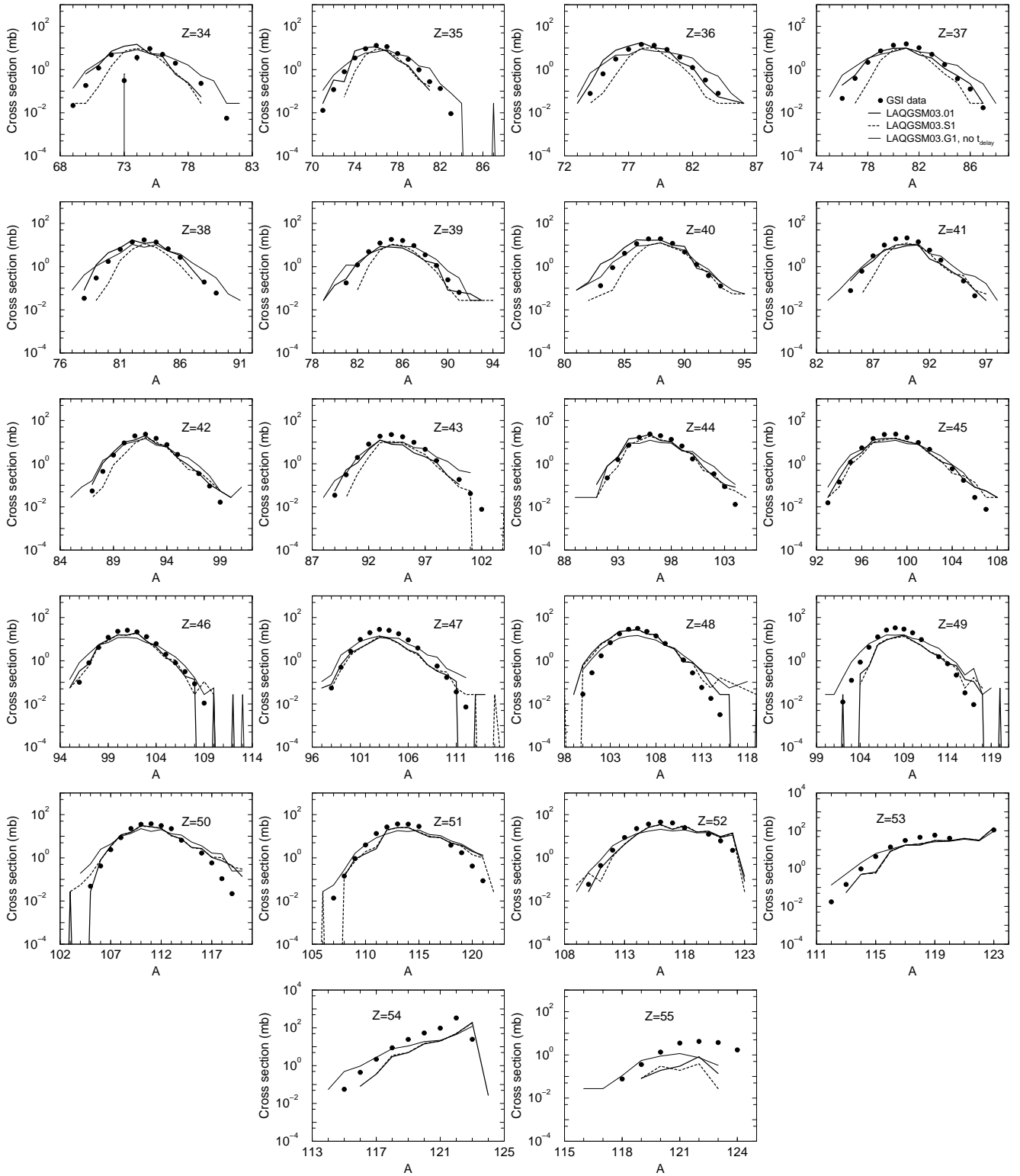


Figure 14: The same as Fig. 13, but for products with Z from 34 to 55.

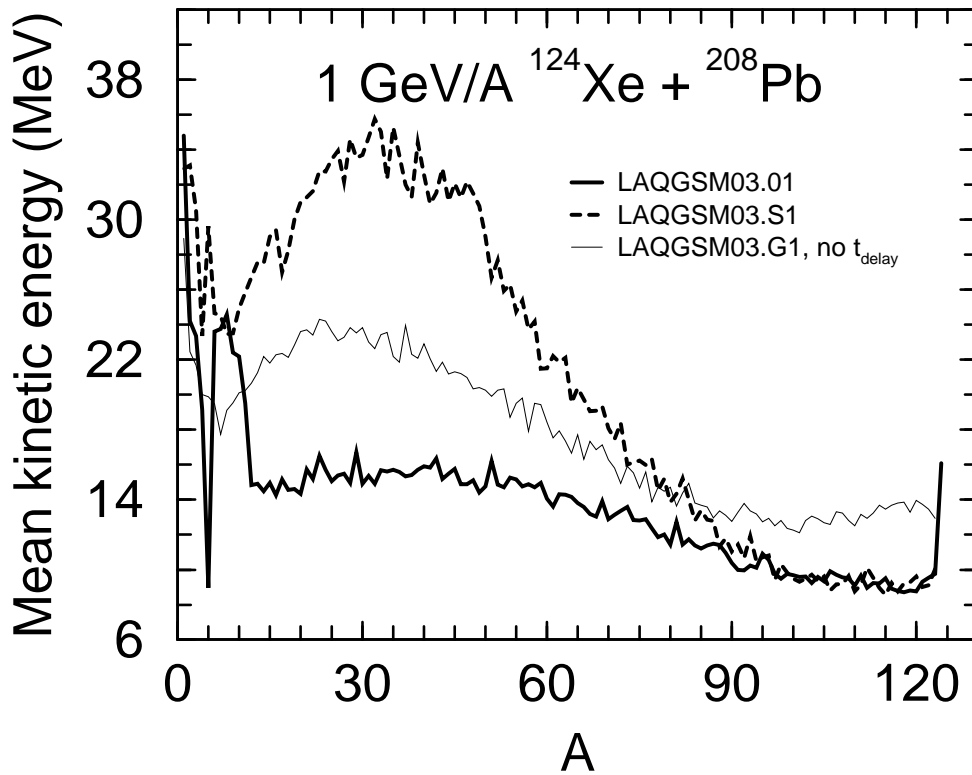
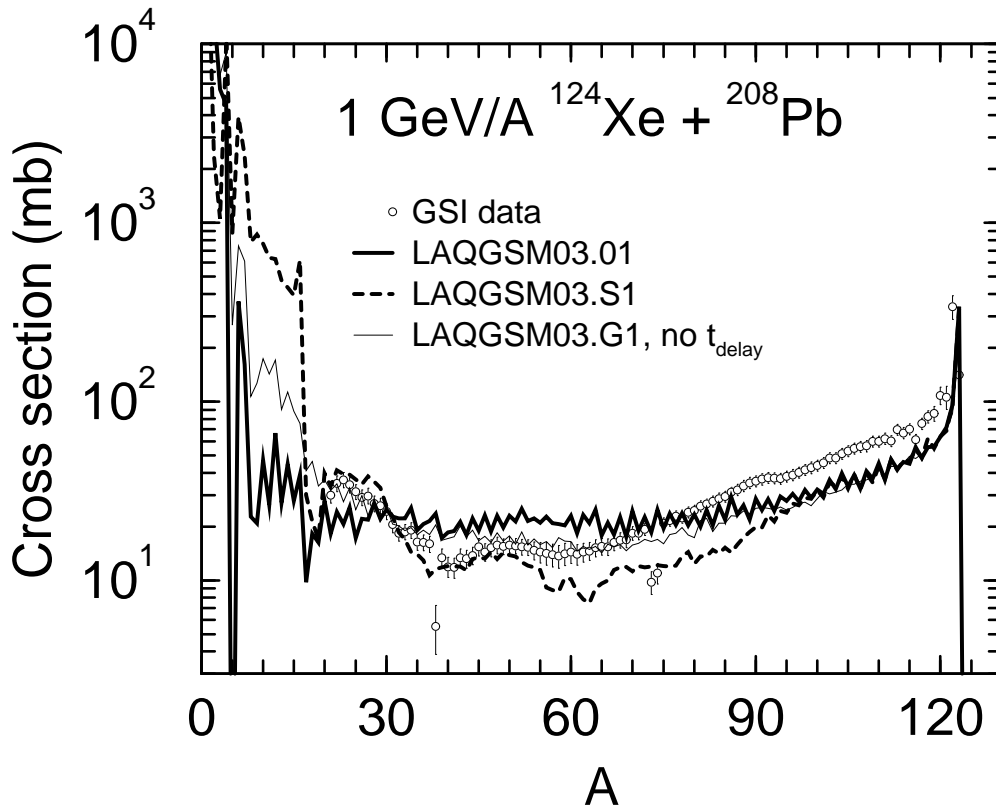


Figure 15: Predictions of LAQGSM03.01, LAQGSM03.S1, and LAQGSM03.G1 for the mass-number distribution of the product yield and the mean kinetic energy of all products from the fragmentation of ^{124}Xe (in the beam system) from the $1 \text{ GeV/A } ^{124}\text{Xe} + ^{208}\text{Pb}$ reaction (lines) compared with available experimental data (circles) [32], as indicated.

Figs. 16 and 17 show results very similar to the ones presented in Figs. 13 and 14, only for another reaction (projectile) measured lately at GSI, 1 GeV/A $^{136}\text{Xe} + \text{Pb}$ [32] (we make all calculations on mono-isotopic ^{208}Pb targets but not on Lead with a natural composition of isotopes as was measured, just as we did for the results presented in Figs. 13–15). The situation for this reaction is very similar to the one for ^{124}Xe shown in Figs. 13 and 14. All comments made above for the ^{124}Xe projectiles (Figs. 13 and 14) are valid and could be repeated here again for reactions of ^{136}Xe (Figs. 16 and 17). ^{124}Xe is the most neutron-deficient stable isotope of Xenon, while ^{136}Xe is the most neutron-rich one; this indicates that our event generators describe equally well reactions involving both neutron-deficient and neutron-rich nuclei.

The only difference between results shown in Figs. 16 and 17 for ^{136}Xe in comparison with results for ^{124}Xe shown in Figs. 13 and 14 is that for ^{136}Xe we perform two sets of calculations with the “G” version of LAQGSM: 1) without taking into account the delay time (results shown with thin solid lines) and 2) with values $t_{\text{delay}} = 75$ and $\sigma_{\text{delay}} = 50$ (results shown with thin dashed lines) for the time-delay parameters of GEMINI. The reason for this additional study for reactions induced by ^{136}Xe is to understand how results by LAQGSM03.G1 depend on the value of the time-delay parameters of GEMINI: These parameters are considered as input parameters of the model and it is up to users to choose them. For instance, for proton-induced reactions, we found [33] that: 1) GEMINI merged with CEM/LAQGSM provides reasonably good results for medium-heavy targets without a fission delay time; 2) For preactinides, we have to use $t_{\text{delay}} = 50\text{--}70$ and $\sigma_{\text{delay}} = 1\text{--}50$, otherwise GEMINI provides too much fission — this may be related to the calculation of fission barriers of preactinides with strong ground-state shell corrections in the version of GEMINI we use; 3) The current version of GEMINI does not work well for actinides.

Our results shown on Figs. 16 and 17 (and on the left panels of Figs. 18 and 19) are only for products of fragmentation of the projectile, ^{136}Xe , just as these reactions are measured at GSI [32]. For such processes, we do not see a big difference between results by LAQGSM03.G1 obtained without taking into account the delay time (thin solid lines) and the ones calculated with $t_{\text{delay}} = 75$ and $\sigma_{\text{delay}} = 50$ (thin dashed lines). This is similar to what we found for proton-induced reactions [33]. As ^{136}Xe is a medium-heavy target, it can be calculated with GEMINI without taking into account the delay time. The situation changes dramatically if we look in the laboratory system at all products from this reaction, just as happens in nature, produced from both the projectile ^{136}Xe and the target ^{208}Pb (see the right panels on Figs. 18 and 19). ^{208}Pb is a preactinide nucleus and has to be calculated with GEMINI using $t_{\text{delay}} = 75$ and $\sigma_{\text{delay}} = 50$, according to our experience gained from studying proton-induced reactions [33] (this is why we choose here these values of t_{delay} and σ_{delay}). From the results presented on plots in the right panels of Figs. 18 and 19, we see that all characteristics of isotopes produced from the target ^{208}Pb calculated with $t_{\text{delay}} = 75$ and $\sigma_{\text{delay}} = 50$ differ significantly from the ones calculated without taking into account the delay time in GEMINI. Unfortunately, these characteristics can not be measured with the GSI technique, and we have no experimental data with which to compare our results.

Just as for reactions induced by ^{124}Xe and protons, from comparison of only the measured [32] product yields from reactions induced by ^{136}Xe (Figs. 16 and 17) with calculations by different versions of LAQGSM it is difficult, if not impossible, to reveal the “real” mechanisms of nuclear reactions contributing to the production of measured isotopes.

1 GeV/A $^{136}\text{Xe} + ^{208}\text{Pb}$

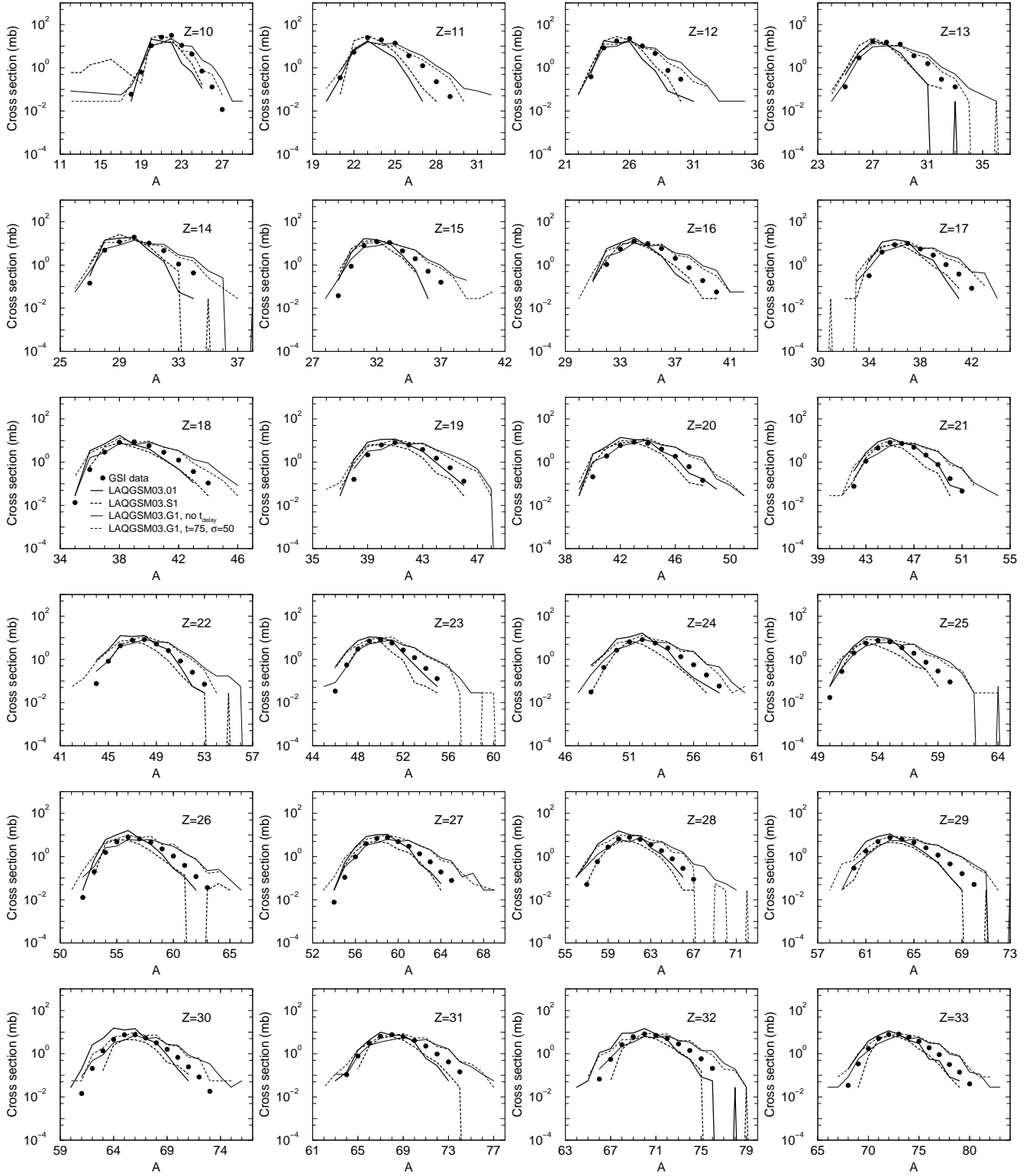


Figure 16: Comparison of LAQGSM03.01, LAQGSM03.S1, and LAQGSM03.G1 results (lines) for the total cross sections (yields) of nuclides with Z from 10 to 33 produced from fragmentation of ^{136}Xe in 1 GeV/A $^{136}\text{Xe} + ^{208}\text{Pb}$ collisions with the GSI data [32] (circles), as indicated. Results by LAQGSM03.G1 calculated without a delay time in GEMINI and with $t_{delay} = 75$ and $\sigma_{delay} = 50$ are shown by solid and dashed thin lines, respectively.

1 GeV/A $^{136}\text{Xe} + ^{208}\text{Pb}$

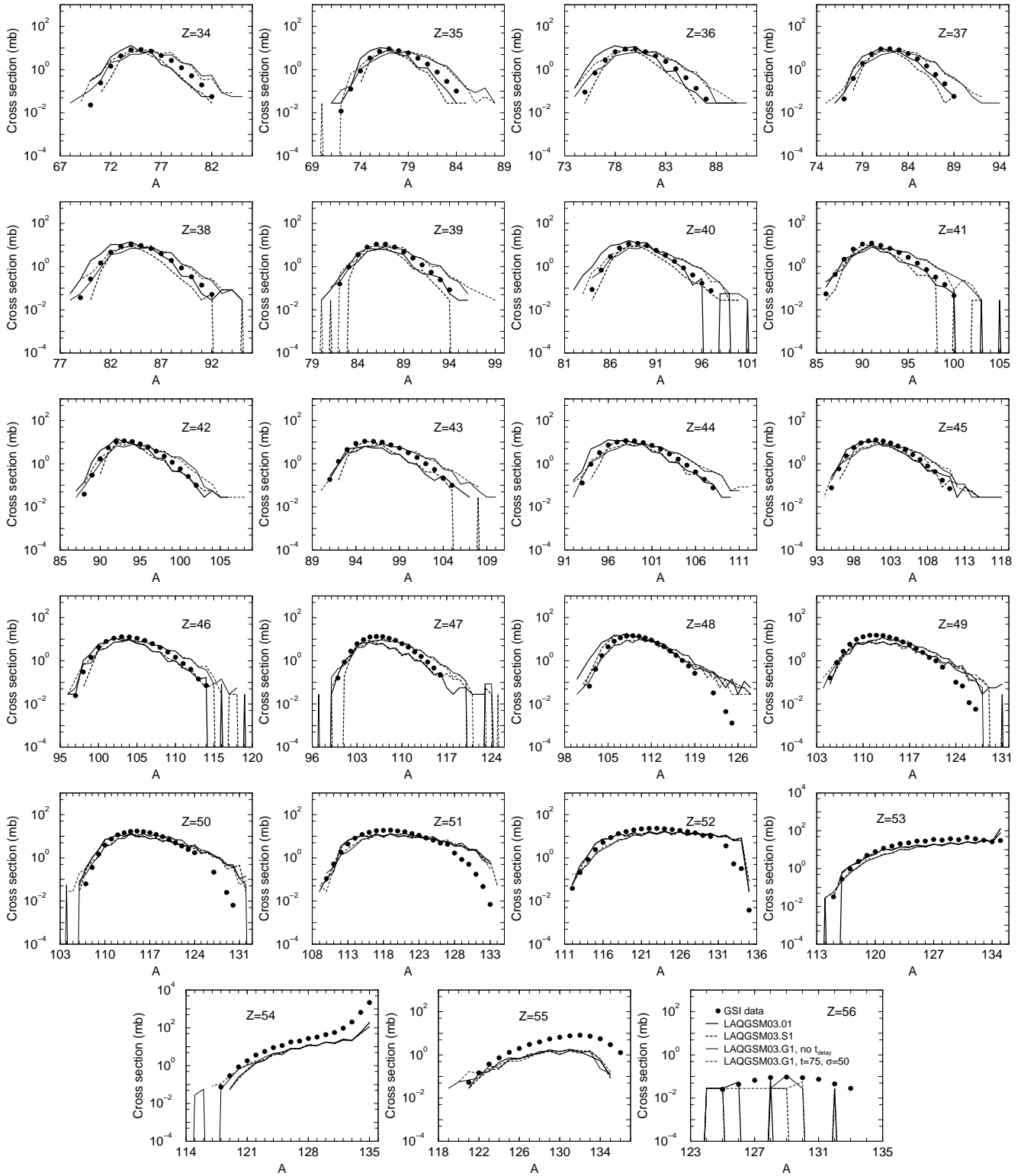


Figure 17: The same as Fig. 16, but for products with Z from 34 to 56.

This is why for reactions induced by ^{136}Xe , we look additionally at several kinematic characteristics like $\langle T_{kin} \rangle$, $\langle v_z \rangle$, $\langle \Theta \rangle$, and $\langle R \rangle$, as we did for proton-induced reactions (Figs. 1, 2, and 5). The left panels of plots in Figs. 18 and 19 show such characteristics (plus, the Z -integrated mass product yield and the cross section for the production of nuclides with $Z = 56$, shown in Fig. 18) calculated in the projectile frame of reference, as all reactions at GSI are measured [32]. There is a big difference between results of the standard version of LAQGSM and of its “G” and “S” versions for the calculated Z -integrated yield of isotopes with $15 < A < 31$, for $\langle T_{kin} \rangle$ of isotopes with $20 < A < 80$, and for $\langle v_z \rangle$, $\langle \Theta \rangle$, and especially for $\langle R \rangle$ of almost all products. Unfortunately, none of these quantities were measured at GSI so we can not identify a specific reaction mechanism based on these results until experimental data are available.

To reveal the effect of angular momentum, L , of the compound nucleus on the kinematic characteristics $\langle v_z \rangle$, $\langle \Theta \rangle$, and $\langle R \rangle$ of the reaction induced by ^{136}Xe , we have performed additional calculations with LAQGSM03.G1 assuming the angular momentum of all compound nuclei is equal to zero. Results of such a modification of LAQGSM03.G1 are shown in Fig. 19 with blue dotted thin lines, to be compared with the thin black solid lines showing results from LAQGSM03.G1 considering the real angular momenta of all compound nuclei (both of these calculations have no delay time in GEMINI). The effect of angular momentum, L , of the compound nuclei on results for $\langle \Theta \rangle$, $\langle R \rangle$, and $\langle v_z \rangle$ calculated by GEMINI in LAQGSM03.G1 is not significant.

Together with results for products from only fragmentation of the projectile calculated in the projectile frame of reference (as all measurements at GSI are done) shown on the left panels of Figs. 18 and 19, on the right panels of the same figures, we show side-by-side similar results calculated in the laboratory system that include isotopes produced from both the projectile and the target. This is the way a reaction really happens in nature, and how a transport code “sees” and uses it in transport calculations from results provided by event generators like LAQGSM. Unfortunately, none of the currently available experimental techniques allow the measurement of all products of heavy-ion reactions, produced from both the projectiles and targets. We can not yet compare the results shown on the right panels with any measurements. However, we find them quite interesting and informative for nuclear applications, including to users and developers of transport codes.

Several phenomenological systematics are presently available in the literature to estimate the cross sections of products from the fragmentation of the projectile in a heavy-ion reaction, with the most advanced and often used, especially at GSI, the EPAX parameterization by K. Sümmerer and B. Blank [34]. Such systematics are very fast and easy to calculate; they are useful and provide quite reliable results to estimate the fragmentation of the projectile in a heavy-ion reaction, especially if experimental data for that reaction, or for a not too different one, were used in deriving the phenomenological systematics. But phenomenological systematics may not provide reliable results for unmeasured reactions that differ significantly from those used in fitting its parameters. In addition, one should be very careful when using systematics like EPAX in applications; the point is that most applications need all products from a reaction, in the laboratory system, while EPAX provides results from only fragmentation of the projectile. So for the reaction $^{136}\text{Xe} + ^{208}\text{Pb}$ discussed here, we can not use EPAX to calculate the inverse reaction $^{208}\text{Pb} + ^{136}\text{Xe}$ adding the results with the ones obtained for the direct Xe+Pb reaction with a hope to obtain all products from this reaction in the laboratory

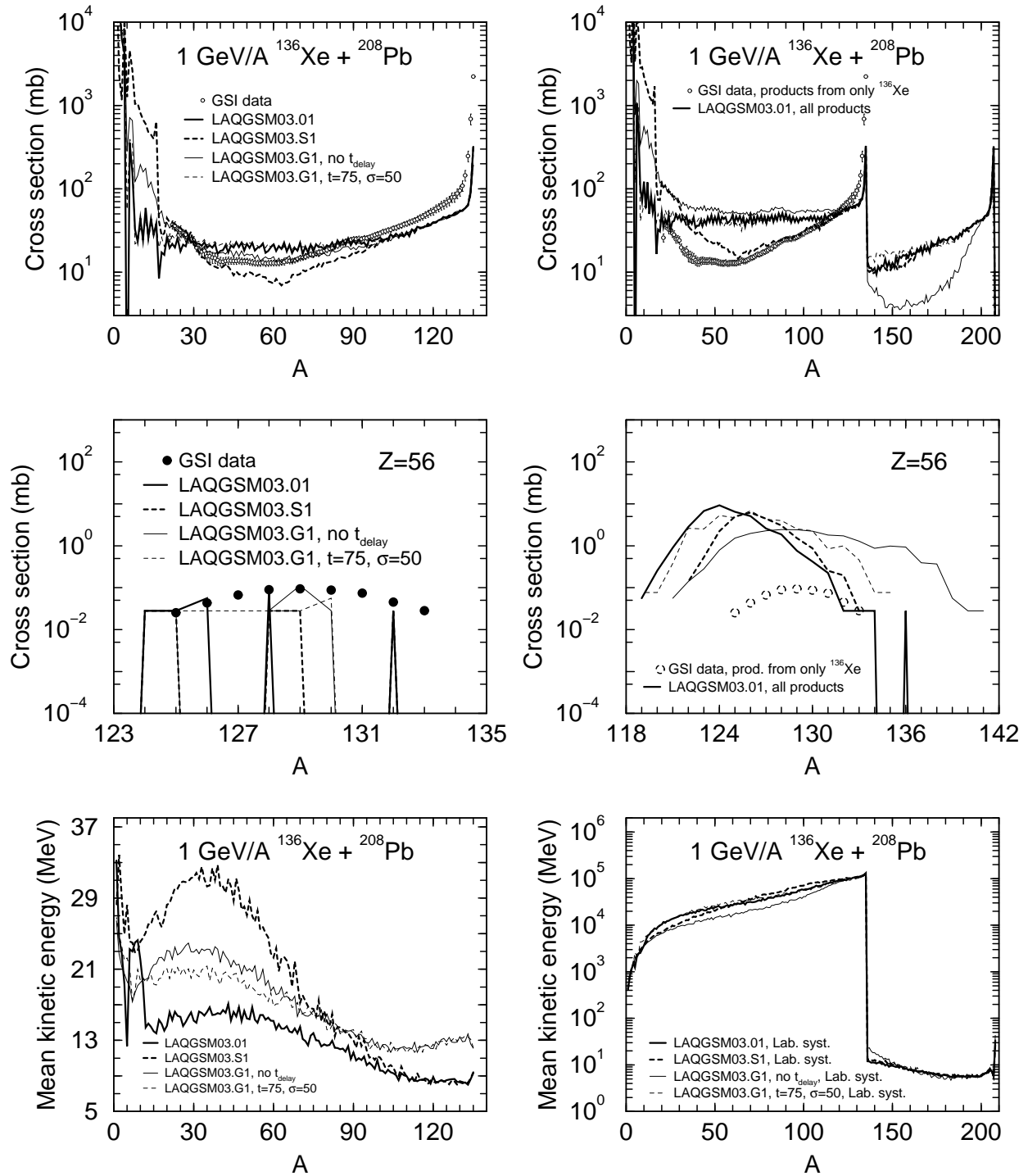


Figure 18: **Left panel:** Predictions of LAQGSM03.01, LAQGSM03.S1, and LAQGSM03.G1 for the Z -integrated mass product yield, cross section of the production of nuclides with $Z = 56$, and the mean kinetic energy of all products from the fragmentation of ^{136}Xe (in the beam system) from the $1 \text{ GeV/A } ^{136}\text{Xe} + ^{208}\text{Pb}$ reaction (lines) compared with available experimental data (circles) [32], as indicated. **Right panel:** The same as on the left panel, but calculated in the laboratory system, as “seen” by a transport code, for all nuclides produced from both the target, ^{136}Xe , and the projectile, ^{208}Pb . Experimental data (dashed circles on the right panel) are measured in the beam system and should be compared only with the results showed on the left panel; this is why they do not agree with the laboratory system results to be used by transport codes shown in the right panel.

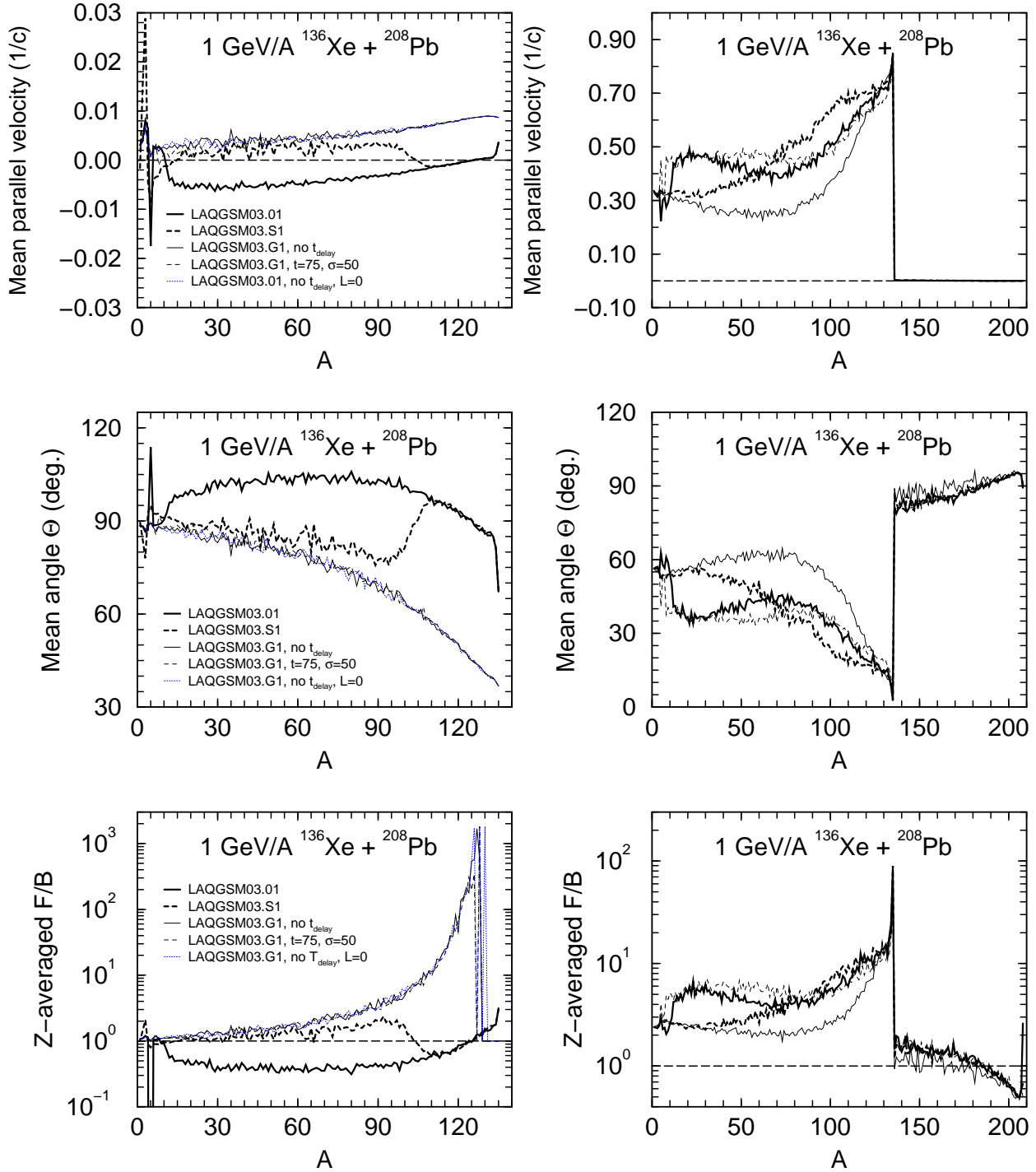


Figure 19: The same as in Fig. 18, but for the mean parallel velocity v_z , mean production angle Θ , Z-averaged A-dependence of the F/B ratio of the forward product cross sections to the backward ones. To reveal the effect of angular momentum, L , of the compound nucleus on results calculated by GEMINI in LAQGSM03.G1, the blue dotted thin lines on the left panel show results obtained assuming $L = 0$ in GEMINI, which should be compared with the results shown on the same plots by thin solid black lines obtained using actual values of L .

system exactly as happens in reality and calculated by an event generator. The point is that we have as products from a heavy-ion reaction not only those from the fragmentation of the projectile but also from the target. Depending on the incident energy of the projectile and on the impact parameter of the colliding nuclei, we may have a significant contribution from intermediate systems produced via the “fusion” of a part of the projectile with a part of the target. Such processes are missed by EPAX, while event generators like our LAQGSM account for them. This is why we need reliable event generators rather than phenomenological systematics in applications. We hope to address this subject in more detail in a later paper.

3. Summary

The recent 660 MeV $p + {}^{129}\text{I}$ and 3.65 GeV $p + {}^{112}\text{Sn}$ JINR activation measurements, the new COSY H, He, Li, and Be production data with 1.2 GeV protons on 13 nuclei from Al to Th, the 300 MeV and 1 GeV $p + {}^{56}\text{Fe}$ data measured at GSI in inverse kinematics, and the new GSI data on fragmentation of Xe from 1 GeV/nucleon ${}^{124}\text{Xe}$ and ${}^{136}\text{Xe} + \text{Pb}$ have been analyzed with the standard versions (that use the Generalized Evaporation Model GEM2 of Furihata to describe evaporation and fission) of our event generators CEM03.01 and LAQGSM03.01, as well as with their “S” (which consider also multifragmentation of compound nuclei produced after the preequilibrium stage of reactions when their excitation energies is above $2 \times A$ MeV) and “G” (which describe evaporation/fission stages of reactions using the fission-like binary-decay model GEMINI of Charity *et al.* instead of using GEM2) modifications. We conclude that from comparison of only these measured product yields with calculations by different versions of our codes it is difficult, if not impossible to uncover the “real” mechanisms of nuclear reactions contributing to the production of measured isotopes. We find that some kinematic characteristics of nuclear reactions like the the mean production angle $\langle \Theta \rangle$, Z-averaged A-dependence of the F/B ratio of the forward product cross sections to the backward ones $\langle R \rangle$, and the mean kinetic energy of all products in the laboratory system, $\langle T_{kin} \rangle$ are described quite differently by GEM2, SMM, and GEMINI, and may be a more powerful tool to understand the “real” mechanisms of fragment production. Such characteristics can not be measured with the GSI inverse kinematics technique or by the activation method used at JINR, but may be measured with some other techniques. We encourage future measurements of such characteristics both for proton-induced and heavy-ion reactions.

We are grateful to Prof. Robert Charity and Dr. Alexander Botvina for generously providing us their GEMINI and SMM codes implemented into the “G” and “S” versions of our event generators. We thank our collaborators, Drs. Arnold Sierk, Richard Prael, and Nikolai Mokhov for their important contributions and support of our work on development the “S” and “G” versions of our codes, as well as for useful discussions of the results. This work was supported by the Advanced Simulating Computing (ASC) Program at the Los Alamos National Laboratory operated by the University of California for the US Department of Energy.

References

- [1] S. G. Mashnik, K. K. Gudima, R. E. Prael, and A. J. Sierk, “Analysis of the GSI A+p and A+A Spallation, Fission, and Fragmentation Measurements with the LANL CEM2k

- and LAQGSM Codes,” *Proc. TRAMU@GSI*, GSI-Darmstadt, Germany, 2003, ISBN 3-00-012276-1, Eds: A. Kelic and K.-H. Schmidt, <http://www-wnt.gsi.de/tramu/>; E-print: nucl-th/0404018.
- [2] S. G. Mashnik, K. K. Gudima, I. V. Moskalenko, R. E. Prael, and A. J. Sierk, “CEM2k and LAQGSM as Event Generators for Space-Radiation-Shielding and Cosmic-Ray-Propagation Applications,” *Advances in Space Research* **34** (2004) 1288–1296.
- [3] S. G. Mashnik, K. K. Gudima, A. J. Sierk, and R. E. Prael, “Improved Intranuclear Cascade Models for the Codes CEM2k and LAQGSM,” *Proc. Int. Conf. on Nuclear Data for Sci. & Techn. (ND2004)*, September 26 - October 1, 2004, Santa Fe, NM, USA, edited by R. C. Haight, M. B. Chadwick, T. Kawano, and P. Talou, (AIP Conference Proceedings, Volume 769, Melville, New York, 2005), pp. 1188–1192.
- [4] S. G. Mashnik, M. I. Baznat, K. K. Gudima, A. J. Sierk, and R. E. Prael, “CEM03 and LAQGSM03: Extension of the CEM2k+GEM2 and LAQGSM Codes to Describe Photo-Nuclear Reactions at Intermediate Energies (30 MeV to 1.5 GeV),” *Journal of Nuclear and Radiochemical Science* **6** (2005) A1–A19.
- [5] K. K. Gudima, S. G. Mashnik, and V. D. Toneev, “Cascade-Exciton Model of Nuclear Reactions,” *Nucl. Phys.* **A401** (1983) 329–361.
- [6] Konstantin K. Gudima, Stepan G. Mashnik, and Arnold J. Sierk, “User Manual for the code LAQGSM,” LANL Report LA-UR-01-6804, Los Alamos (2001), <http://lib-www.lanl.gov/la-pubs/00818645.pdf>.
- [7] S. G. Mashnik, K. K. Gudima, M. I. Baznat, A. J. Sierk, R. E. Prael, and N. V. Mokhov, “CEM03.01 and LAQGSM03.01 Versions of the Improved Cascade-Exciton Model (CEM) and Los Alamos Quark-Gluon String Model (LAQGSM) Codes,” LANL Report LA-UR-05-2686, Los Alamos (2005).
- [8] S. G. Mashnik, A. J. Sierk, K. K. Gudima, M. I. Baznat, “CEM03 and LAQGSM03—New Modeling Tools for Nuclear Applications,” *Proc. European Physical Society 19th Nuclear Physics Division Conference **New Trends in Nuclear Physics Applications and Technology (NPDC19)***, Pavia, Italy, September 5–9, 2005, LANL Report LA-UR-05-8130, Los Alamos (2005), E-print: nucl-th/0510070, *Journal of Physics: Conference Series*, in press.
- [9] Stepan G. Mashnik, Konstantin K. Gudima, Arnold J. Sierk, Mircea I. Baznat, and Nikolai V. Mokhov, “CEM03.01 User Manual,” LANL Report LA-UR-05-7321, Los Alamos (2005).
- [10] S. G. Mashnik, K. K. Gudima, M. I. Baznat, A. J. Sierk, R. E. Prael, and N. V. Mokhov, “CEM03.S1, CEM03.G1, LAQGSM03.S1, and LAQGSM03.G1 Versions of CEM03.01 and LAQGSM03.01 Event-Generators,” LANL Report LA-UR-06-1764, Los Alamos (2006).
- [11] J. P. Bondorf, A. S. Botvina, A. S. Iljinov, I. N. Mishustin, and K. Sneppen, “Statistical Multifragmentation of Nuclei,” *Phys. Rep.* **257** (1995) 133–221.
- [12] A. S. Botvina, A. S. Iljinov, I. N. Mishustin, J. P. Bondorf, R. Donangelo, and K. Sneppen, “Statistical Simulation of the Break-up of Highly Excited Nuclei,” *Nucl Phys.* **A475** (1987) 663–686.
- [13] A. S. Botvina, K. K. Gudima, A. S. Iljinov, and I. N. Mishustin. “Multifragmentation of Highly-Excited Nuclei in Nucleus-Nucleus Collisions at Intermediate Energies,” *Yad. Fiz.* **57** (1994) 667–674 [*Phys. At. Nucl.* **57** (1994) 628–635].

- [14] A. S. Botvina, A. S. Iljinov, and I. N. Mishustin, “Multifragmentation Break-up of Nuclei by Intermediate-Energy Protons,” *Nucl. Phys.* **A507** (1990) 649–674.
- [15] A. S. Botvina, A. S. Iljinov, and I. N. Mishustin, “Multifragmentation of Nuclei at Excitation-Energies Approximately 10 MeV/Nucleon,” *Yad. Fiz.* **42** (1985) 1127–1137 [*Sov. J. Nucl. Phys.* **42** (1985) 712–718].
- [16] S. Furihata, “Statistical Analysis of Light Fragment Production from Medium Energy Proton-Induced Reactions,” *Nucl. Instr. Meth. B* **171** (2000) 252–258; “The Gem Code—the Generalized Evaporation Model and the Fission Model,” *Proc. MC2000, Lisbon, Portugal, 2000*, edited by A. Kling, F. J. C. Barão, M. Nakagawa, L. Távora, and P. Vaz, Springer, Berlin, (2001), pp. 1045–1050; *The Gem Code Version 2 Users Manual*, Mitsubishi Research Institute, Inc., Tokyo, Japan (November 8, 2001).
- [17] S. Furihata, K. Niita, S. Meigo, Y. Ikeda, and F. Maekawa, “The Gem Code—a Simulation Program for the Evaporation and Fission Process of an Excited Nucleus,” *JAERI-Data/Code 2001-015*, JAERI, Tokai-mura, Naka-gam, Ibaraki-ken, Japan (2001).
- [18] Shiori Furihata, “Development of a Generalized Evaporation Model and Study of Residual Nuclei Production,” Ph.D. thesis, Tohoku University, March, 2003; S. Furihata and T. Nakamura, “Calculation of Nuclide Production from Proton Induced Reactions on Heavy Targets with INC/GEM,” *J. Nucl. Sci. Technol. Suppl.* **2** (2002) 758–761.
- [19] L. G. Sobotka, M. A. McMahan, R. J. McDonald, C. Signarbieux, G. J. Wozniak, M. L. Padgett, J. H. Gu, Z. H. Liu, Z. Q. Yao, and L. G. Moretto, “Compound-Nucleus Decay along the Mass-Asymmetry Coordinate and the Role of the Businaro-Gallone Point,” *Phys. Rev. Lett.* **53** (1984) 2004–2007.
- [20] R. J. Charity, M. A. McMahan, G. J. Wozniak, R. J. McDonald, L. G. Moretto, D. G. Sarantites, L. G. Sobotka, G. Guarino, A. Pantaleo, L. Fiore, A. Gobbi, and K. D. Hildenbrand, “Systematics of Complex Fragment Emission in Niobium-Induced Reactions,” *Nucl. Phys. A* **483** (1988) 371–405.
- [21] R. J. Charity, D. R. Bowman, Z. H. Liu, R. J. McDonald, M. A. McMahan, G. L. Wozniak, L. G. Moretto, S. Bardley, W. L. Kenoe, and A. C. Mignerey, “Emission of Complex Fragments from Highly Excited Systems Produced in $^{93}\text{Nb}+^9\text{Be}$ and ^{27}Al Reactions at $E/A = 25.4$ and 30.3 MeV,” *Nucl. Phys.* **A476** (1988) 516–544.
- [22] R. J. Charity, “ $N-Z$ Distributions of Secondary Fragments and the Evaporation Attractor Line”, *Phys. Rev. C* **58** (1988) 1073–1077.
- [23] R. J. Charity, L. G. Sobotka, J. Cibor, K. Hagel, M. Murray, J. B. Natowitz, R. Wada, Y. El Masri, D. Fabris, G. Nebbia, G. Viesti, M. Cinausero, E. Fioretto, G. Prete, A. Wagner, and H. Xu, “Emission of Unstable Clusters from Yb Compound Nuclei,” *Phys. Rev. C* **63** (2001) 024611; <http://www.chemistry.wustl.edu/~rc/gemini/>.
- [24] J. Adam, A. Balabekyan, V. S. Barashenkov, V. P. Dzhelepov, S. A. Gustov, V. P. Filinova, V. G. Kalinnikov, M. I. Krivopustov, I. V. Mirokhin, V. S. Pronskikh, A. A. Solnyshkin, V. I. Stegailov, V. M. Tsoupko-Sitnikov, J. Mrazek, R. Brandt, W. Westmeier, R. Odoj, S. G. Mashnik, R. E. Prael, K. K. Gudima, and M. I. Baznat, “Study of Product Production from Proton-Induced Reaction on the ^{129}I Target at Proton Energy 660 MeV,” *Pis'ma v EChAYa*, **1**, No. 4 [121] (2004) 53–64 [*Particles and Nuclei, Letters*, **1**, No. 4, 2004].
- [25] Carmen Villagrasa-Canton, “Etude de la Production des Noyaux Résiduels dans la Réaction de Spallation $\text{Fe} + \text{p}$ à 5 Énergies (300–1500 MeV/A) et Application au Calcul de Dommage sur une Fenêtre de Système Hybride,” PhD Thesis, Université de Paris

- XI Orsay, December 5, 2003, <http://www-w2k.gsi.de/charms/theses.htm>, and private communication from Dr. Villagrasa to SGM, March 11, 2004.
- [26] C. Villagrasa, A. Boudard, J.-E. Ducret, B. Fernandez, S. Leray, C. Volant, W. Wlazole, P. Armbruster, T. Enqvist, F. Hammache, K. Helariutta, B. Jurado, M. V. Ricciardi, K.-H. Schmidt, K. Sümmerer, F. Vivès, O. Yordanov, L. Audouin, L. Ferran, F. Rejmund, C. Stéphan, L. Tassan-Got, J. Benlliure, E. Casarejos, M. Fernandez, J. Pereira, S. Czajkowski, D. Karamanis, M. Pravikoff, J. George, R. A. Mewaldt, N. Yanazak, M. Wiedenbeck, J. Connel, T. Faestermann, A. Heinz, A. Junghans, “Measurement of Residual Nucleus Cross Sections and Recoil Energies in p+Fe Collisions at 300, 500, 750, 1000, and 1500 MeV,” Proc. ND2004, September 26–October 1, 2004, Santa Fe, NM, USA, edited by R. C. Haight, M. B. Chadwick, T. Kawano, and P. Talou, (AIP Conference Proceedings, Volume 769, Melville, New York, 2005), pp. 842–845.
- [27] Paolo Napolitani, “New Findings on the Onset of Thermal Disassembly in Spallation Reactions,” PhD Thesis, University Paris XI Orsay, IPNO-T-04-14, September 24, 2004, <http://www-w2k.gsi.de/charms/theses.htm>, and private communication from Dr. Napolitani to SGM, 2004.
- [28] P. Napolitani, K.-H. Schmidt, A. S. Botvina, F. Rejmund, L. Tassan-Got, and C. Villagrasa, “High-Resolution Velocity Measurements on Fully Identified Light Nuclides Produced in $^{56}\text{Fe} + \text{Hydrogen}$ and $^{56}\text{Fe} + \text{Titanium}$ Systems,” Phys. Rev. C **70** (2004) 054607.
- [29] A. R. Balabekyan, A. S. Danagulyan, J. R. Drnoyan, G. H. Hovhannisyan, J. Adam, V. G. Kalinnikov, M. I. Krivopustov, V. S. Pronskikh, V. I. Stegailov, A. A. Solnyshkin, P. Chaloun, V. M. Tsoupkov-Sitnikov, S. G. Mashnik, and K. K. Gudima, “Large Formation of Light Isotopes by Protons and Deuterons of 3.65 GeV/nucleon on Separated Tin Isotopes,” LANL Report LA-UR-05-4676 (2005); E-print: nucl-ex/0506024; to be published in Yadernaya Fizika [Physics of Atomic Nuclei], 2006.
- [30] G. Roy, L. Greeniaus, G. A. Moss, D. A. Hutcheon, R. Liljestrang, R. M. Woloshyn, D. H. Boal, A. W. Stetz, K. Aniol, A. Willis, N. Willis, and R. McCamis, “Inclusive Scattering of Protons on Helium, Nickel, and Tantalum at 500 MeV,” Phys. Rev. C **23** (1981) 16711–1678.
- [31] C.-M. Herbach, D. Hilscher, U. Jahnke, V. G. Tishchenko, J. Galin, A. Letourneau, A. Péghaire, D. Filges, F. Goldenbom, L. Penkowski, W. U. Schröder, and J. Töke, “Charged-Particle Evaporation and Pre-Equilibrium Emission in 1.2 GeV Proton-Induced Spallation Reactions,” Nucl. Phys. **A765** (2006) 426–463.
- [32] Daniela Henzlová, “Systematic Investigation of the Isotopic Distributions Measured in the Fragmentation of ^{124}Xe and ^{136}Xe Projectiles,” PhD Thesis, Czech Technical University in Prague, October 2005, <http://www-w2k.gsi.de/charms/theses.htm>.
- [33] M. I. Baznat, K. K. Gudima, S. G. Mashnik, and R. E. Prael, “Merging the CEM2k and LAQGSM Codes with GEMINI,” LANL Report LA-UR-05-0559, Los Alamos (2005), E-print: nucl-th/0501075, v2, November 2, 2005.
- [34] K. Sümmerer and B. Blank, “Modified Empirical Parameterization of Fragmentation Cross Sections,” Phys. Rev. C **61** (2000) 034607; K. Sümmerer, “Fragmentation Cross Sections Outside the Limiting-Fragmentation Regime,” Nucl. Instr. and Meth. B **204** (2003) 278–281; <http://www-w2k.gsi.de/charms/software.htm>.